arXiv:1702.03417v1 [stat.ME] 11 Feb 2017

On a spiked model for large volatility matrix estimation from noisy high-frequency data

Keren Shen
Department of Statistics and Actuarial Science
The University of Hong Kong
Jianfeng Yao
Department of Statistics and Actuarial Science
The University of Hong Kong
and
Wai Keung Li
Department of Statistics and Actuarial Science
The University of Hong Kong

February 14, 2017

Abstract

Recently, inference about high-dimensional integrated covariance matrices (ICVs) based on noisy high-frequency data has emerged as a challenging problem. In the literature, a pre-averaging estimator (PA-RCov) is proposed to deal with the microstructure noise. Using the large-dimensional random matrix theory, it has been established that the eigenvalue distribution of the PA-RCov matrix is intimately linked to that of the ICV through the Marčenko-Pastur equation. Consequently, the spectrum of the ICV can be inferred from that of the PA-RCov. However, extensive data analyses demonstrate that the spectrum of the PA-RCov is *spiked*, that is, a few large eigenvalues (spikes) stay away from the others which form a rather continuous distribution with a density function (bulk). Therefore, any inference on the ICVs must take into account this spiked structure. As a methodological contribution, we propose a spiked model for the ICVs where spikes can be inferred from those of the available PA-RCov matrices. The consistency of the inference procedure is established and is checked by extensive simulation studies. In addition, we apply our method to the real data from the US and Hong Kong markets. It is found that our model clearly outperforms the existing one in predicting the existence of spikes and in mimicking the empirical PA-RCov matrices.

Keywords: integrated covariance matrix, pre-averaging, random matrix theory, spiked covariance matrix

1 Introduction

Modeling and forecasting covariance matrices of asset returns play a crucial role in many financial applications, such as portfolio allocation and asset pricing. With the availability of intraday financial data, it becomes possible to estimate the so-called *integrated covariance matrix* (ICV) of asset returns using the *realized covariance matrix* which is directly attainable from the high-frequency data (Andersen et al., 2003, Barndorff-Nielsen and Shephard, 2004 and Barndorff-Nielsen et al., 2011). More precisely, suppose there are p stocks whose log-price processes are denoted by $\mathbf{X}_t = (X_t^1, \cdots, X_t^p)^T$. A commonly used model for $\mathbf{X}_t$ is the following high-dimensional diffusion process:

$$d\mathbf{X}_t = \boldsymbol{\mu}_t dt + \boldsymbol{\Theta}_t d\mathbf{W}_t, \quad t \in [0,1],$$

where $\boldsymbol{\mu}_t = (\mu_t^1, \cdots, \mu_t^p)^T$ is a p-dimensional drift process, $\boldsymbol{\Theta}_t$ is a $p \times p$ co-volatility matrix, and $(\mathbf{W}_t)$ is a p-dimensional standard Brownian motion. The ICV is defined as

$$\text{ICV} := \int_0^1 \boldsymbol{\Theta}_t \boldsymbol{\Theta}_t^T dt.$$

In practice, the intraday prices are always contaminated by the market microstructure noise. As a matter of fact, we observe, instead of the underlying process $(\mathbf{X}_{t_i})$, a noisy version:

$$\mathbf{Y}_{t_i} = \mathbf{X}_{t_i} + \boldsymbol{\varepsilon}_i, \quad i = 1, \cdots, n,$$

where $\mathbf{Y}_{t_i} = (Y_i^1, \cdots, Y_i^p)^T$ denotes the observations, and $\boldsymbol{\varepsilon}_i = (\varepsilon_i^1, \cdots, \varepsilon_i^p)^T$ denotes the noise, which is i.i.d. with mean $\mathbf{0}$ and covariance matrix $\boldsymbol{\Sigma}_e$, and is independent of $(\mathbf{X}_{t_i})$.

To filter out the effect of the noise, it is recommended in the literature to pre-average the data as follows (Christensen et al., 2010). Choose a window length $k_n = \lfloor \theta\sqrt{n} \rfloor$ where $\theta \in (0, \infty)$ and a function $g(x) = \min(x, 1-x)$ on $[0,1]$. For any process $\mathbf{V} = (\mathbf{V}_t)_{t \geq 0}$, consider the increments (return)

$$\Delta_i^n \mathbf{V} = \mathbf{V}_{i/n} - \mathbf{V}_{(i-1)/n}, \text{ for } i = 1, \cdots, n.$$

The pre-averaged process is

$$\bar{\mathbf{V}}_i^n = \sum_{j=1}^{k_n - 1} g(\frac{j}{k_n}) \Delta_{i+j}^n \mathbf{V}, \text{ for } i = 0, \cdots, n - k_n + 1.$$

Therefore, the observed return based on the pre-averaging price is

$$\bar{\mathbf{Y}}_i^n = \bar{\mathbf{X}}_i^n + \bar{\boldsymbol{\varepsilon}}_i^n.$$

Then, the *pre-averaging realized covariance matrix* (PA-RCov) is defined as

$$\text{PA-RCov} := \frac{n}{n-k_n+2}\frac{1}{\psi_2 k_n}\sum_{i=0}^{n-k_n+1}(\bar{\mathbf{Y}}_i^n)(\bar{\mathbf{Y}}_i^n)^T,$$

where $n/(n-k_n+2)$ is a finite sample correction and ψ_2 is a correction function related to function g. In low dimensional case when the number of the stocks p is small compared to the sample size n, it can be proved that the PA-RCov is a consistent estimator of the ICV under an appropriate choice of the window length k. However, when the number p becomes large, the PA-RCov is no longer a good estimator even in the simplest case when the co-volatility process remains unchanged. In particular, the spectrum of the PA-RCov will deviate from that of the ICV.

A few papers have appeared recently in the literature to deal with this challenging problem of estimation of high-dimensional ICV matrices. Wang and Zou (2010) use thresholding and banding regularization techniques to estimate the ICV under sparsity or decay assumptions on the ICV. Tao et al. (2011) use a similar approach to construct the realized covariance matrix and incorporate low-frequency dynamics in their modeling. However, few work exists to deal with non-sparse ICV matrices while the microstructure noise is present. In a recent paper, Xia and Zheng (2014) propose a new pre-averaging estimator for the spectrum of such *non-sparse* ICV matrices. To make the statistical inference of ICV possible, $(\mathbf{X}_t)$ is required to belong to Class $\mathcal{C}$ such that $\boldsymbol{\Theta}_t = \gamma_t\boldsymbol{\Lambda}$ for some constant matrix $\boldsymbol{\Lambda}$ and (γ_t) is a càdlàg function from $[0,1]$ to $\mathbb{R}$. Then, the ICV can be written as

$$\text{ICV} = \int_0^1 \gamma_t^2 dt \cdot \breve{\boldsymbol{\Sigma}}, \quad \text{where } \breve{\boldsymbol{\Sigma}} = \boldsymbol{\Lambda}\boldsymbol{\Lambda}^T.$$

In other words, (γ_t) serves as a time-varying scaling of the base ICV matrix $\breve{\boldsymbol{\Sigma}}$. Notice that here the dynamic of the volatility process $\boldsymbol{\Theta}_t$ depends on one scalar function γ_t only. However, a fully general model $\boldsymbol{\Theta}_t = (\theta_{ij}(t))$ using p^2 functions would be impossible to identify. Furthermore, we may later extend such setting to a greater freedom as follows. Stocks are naturally grouped to, say s sectors($s \ll p$). With p_k stocks in kth sector($p_1 +$

$\cdots + p_s = p$), we may allow a different base volatility matrix $\mathbf{\Lambda}_k(p_k \times p_k)$ for each sector $k(1 \leq k \leq s)$ associated to a specific dynamic function γ_{kt}. The overall volatility matrix becomes $\mathbf{\Theta}_t = \text{diag}(\gamma_{kt}\mathbf{\Lambda}_k)_{1\leq k\leq s}$ and the corresponding integrated covariance matrix becomes $\text{ICV} = \text{diag}(\int_0^1 \gamma_{kt}^2 dt \cdot \mathbf{\Lambda}_k\mathbf{\Lambda}_k^T)_{1\leq k\leq s}$. Nevertheless, in this paper, we focus on the simplest setting and extension to the block-diagonal case above is not difficult. To construct consistent estimator for the above ICV, Xia and Zheng (2014) consider a slightly different scheme of the pre-averaging estimator. Choose a window length k and group the intervals $[(i-1)/n, i/n]$, $i = 1, \cdots, 2k \cdot \lfloor n/(2k) \rfloor$ into $m = \lfloor n/(2k) \rfloor$ pairs of non-overlapping windows. For any process $\mathbf{V} = (\mathbf{V}_t)_{t\geq 0}$, let

$$\Delta\mathbf{V}_i = \mathbf{V}_{i/n} - \mathbf{V}_{(i-1)/n}, \bar{\mathbf{V}}_i = \frac{1}{k}\sum_{j=0}^{k-1} \mathbf{V}_{((i-1)k+j)/n}, \text{ and } \Delta\bar{\mathbf{V}}_{2i} = \bar{\mathbf{V}}_{2i} - \bar{\mathbf{V}}_{2i-1}.$$

Then, the following PA-RCov matrix is considered:

$$\mathcal{B}_m := 3\frac{\sum_{i=1}^m |\Delta\bar{\mathbf{Y}}_{2i}|^2}{m} \sum_{i=1}^m \frac{\Delta\bar{\mathbf{Y}}_{2i}(\Delta\bar{\mathbf{Y}}_{2i})^T}{|\Delta\bar{\mathbf{Y}}_{2i}|^2}, \tag{1}$$

where for any vector $\mathbf{v}$, $|\mathbf{v}|$ is its Euclidean norm. In this paper, we will use the version of Xia and Zheng (2014) for the PA-RCov $\mathcal{B}_m$. Recall that the *empirical spectral distribution* (ESD) of a symmetric matrix $\mathbf{A}$ of size $p \times p$ is the probability distribution

$$F^{\mathbf{A}} = \frac{1}{p}\sum_{j=1}^p \delta_{\lambda_j},$$

where $(\lambda_j)_{1\leq j\leq p}$ are the eigenvalues of $\mathbf{A}$, and δ_x is the Dirac mass. A key ingredient here is that the ESDs of $\mathcal{B}_m$ and the ICV are related in the high-dimensional case. Precisely, when $p \to \infty$ and $p/m \to y \in (0, \infty)$, the ESDs of the ICV and $\mathcal{B}_m$ converge almost surely to probability distributions F^{ICV} and $F^{\mathcal{B}_\infty}$, respectively. Moreover, the Stieltjes transform of $F^{\mathcal{B}_\infty}$, denoted by $s_{\mathcal{B}_\infty}(z)$, satisfies the Marčenko-Pastur equation associated with F^{ICV}. As a result, the spectrum of the ICV can be inferred from that of $\mathcal{B}_m$ using this equation. For instance, assume the limiting spectral distribution of the ICV is of the form of a weighted sum of point masses

$$F^{\text{ICV}} = \sum_{k=1}^N w_k \delta_{x_k},$$

where $\{x_1 < x_2 < \cdots < x_N\}$ is a grid of pre-determined points, and w_k's are weights to be estimated from the PA-RCov $\mathcal{B}_m$. Precisely, in the Marčenko-Pastur equation linking F^{ICV}

and $F^{\mathcal{B}_\infty}$, $F^{\mathcal{B}_\infty}$ is replaced by $F^{\mathcal{B}_m}$ which is available, and the weights $\{w_k\}$ are selected by solving the equation. Note that as a consequence, this estimator of the ICV provides the estimated weights $\{\hat{w}_k\}$ over the grid points $\{x_1 < x_2 < \cdots < x_N\}$, and these are not exactly the set of eigenvalues of the ICV. For more information about the Stieltjes transform and the Marčenko-Pastur equation, please refer to Bai and Silverstein (2010).

From the Marčenko-Pastur equation, it is known that the eigenvalues of the PA-RCov have a finite support, made of a finite number of intervals. However, Laloux et al. (2000) and Plerou et al. (2002) find that the sample covariance matrix of asset returns always exhibits some large eigenvalues, or *spikes*, separated from the core spectrum (*bulk*). They also find that the eigenvectors corresponding to these spiked eigenvalues are relatively stable and carry meaningful economical information. For example, the largest eigenvalue corresponds to the largest potential risk of the portfolio. More importantly, our empirical study finds that the spectrum of the PA-RCov also comprises a spike part and a bulk part. For illustration, consider an example of 92 stocks extracted from the S&P 100 index. On September 29th, 2008, the ESD of $\mathcal{B}_m$ made with its 92 eigenvalues is plotted in Figure 1.

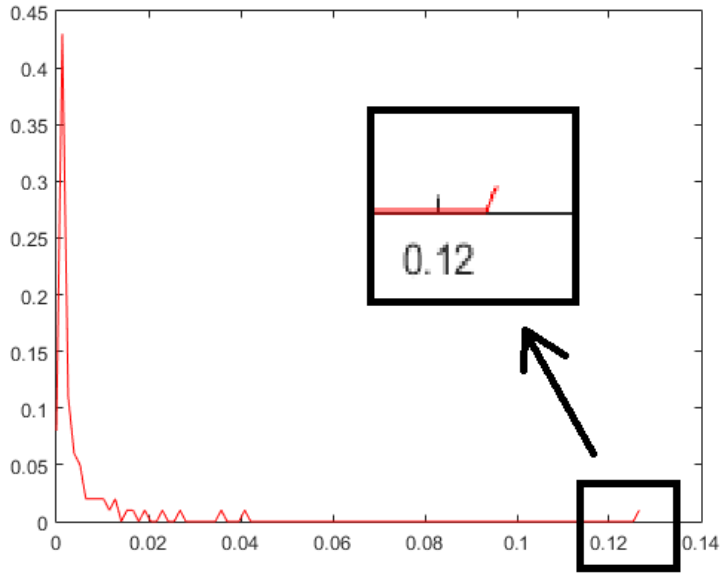

Figure 1: The ESD of the pre-averaging estimator $\mathcal{B}_m$ on September 29th, 2008

From Figure 1, it is seen that the majority of the 92 eigenvalues concentrate in the range

$[0, 0.02]$ while there is a large eigenvalue near 0.13, far away from the bulk part. Naturally, there should be a corresponding spike for the ICV, which is ought to be tackled separately from the bulk part. Notice that there might be other spikes between the bulk range $[0, 0.02]$ and the largest eigenvalue, though a precise inference on this question is yet to be defined (see Section 4.1.1 for details). Nevertheless, the model proposed by Xia and Zheng (2014) ignores such spiked structure in the spectrum of the ICV as their estimator makes no distinction between the spikes which are large and isolated eigenvalues and the bulk which typically has a continuous density. In this paper, we propose a spiked model for the ICV which is capable of taking into account both the spiked eigenvalues and the bulk component in its spectrum. Such spiked structure in the ICV will lead to an associated spiked structure in the spectrum of the observed PA-RCov $\mathcal{B}_m$ and as demonstrated in Figure 1, this matches better the reality.

The spiked model is first introduced by Johnstone (2001) where all eigenvalues of the population covariance matrix are unit except a fixed small number of them. Baik and Silverstein (2006) consider a more general spiked model with complex or real and not necessarily Gaussian random variables. Later, Paul (2007) and Bai and Yao (2008) establish the central limit theorem for extreme sample eigenvalues generated by spiked eigenvalues. Moreover, Bai and Yao (2012) consider a *generalized spiked eigenvalue model* with a much extended structure of spiked eigenvalues. Other related works include Passemier and Yao (2014) and Yao et al. (2015). The above spiked models all assume that the observed vectors are purely drawn from the multivariate distributions. On the contrary, we construct a spiked model in the setting of Xia and Zheng (2014) where the observed returns are contaminated with finite variation and microstructure noise parts. In this paper, we establish the asymptotic relationship between the spiked eigenvalues of the PA-RCov and those of the ICV, by an equation similar to that in the generalized spiked model introduced by Bai and Yao (2012). As a result, the spikes of the ICV can be inferred from those of the PA-RCov. The consistency proved in the theorem is also demonstrated by extensive simulation studies. It is found that the asymptotic property holds, in various kinds of situations, where we have one or more spikes, and where the spikes have different magnitudes. In addition, we apply our model to the real data in the US market and the Hong Kong market. We find that our model consistently outperforms the model proposed by Xia and Zheng (2014) in predicting the existence of spikes and in

mimicking the empirical PA-RCov matrices.

In summary, the main contributions of this paper are as follows. To our best knowledge, this is the first paper introducing a spiked model for the realized covariance matrix and the ICV. In addition, we apply the model to analyzing real data, which is not found in Xia and Zheng (2014). We also report some interesting findings in the empirical study, for example, the magnitude of the largest eigenvalue of the PA-RCov may be a potential leading factor of the volatility of the return series. Finally, we show in detail how and why the model of Xia and Zheng (2014) fails to capture the truth of spikes.

The rest of the paper is organized as follows. Section 2 introduces our new spiked model and establishes the main theorem on the consistency of the estimated spikes. This consistency is checked through extensive simulation studies in Section 3. We apply our model to the real data in Section 4 where we compare our model with that of Xia and Zheng (2014). Section 5 concludes.

2 A spiked model for the ICV

We set some notations that will be used throughout the paper. For any real matrix $\mathbf{A}$, $\|\mathbf{A}\| = \sqrt{\lambda_{\max}(\mathbf{A}\mathbf{A}^T)}$ denotes its spectral norm, where $\lambda_{\max}$ denotes the largest eigenvalue. Moreover, $\mathbf{A}_i$ denotes the ith column of $\mathbf{A}$ and a_i^j denotes the jth entry in $\mathbf{A}_i$. Finally, Γ_μ denotes the support of a finite measure μ on $\mathbb{R}$.

As said in Introduction, we separate the spectrum of the ICV into a bulk part and a spikes part. Specifically, we assume that the constant matrix component of the ICV, $\breve{\mathbf{\Sigma}} = \mathbf{\Lambda}\mathbf{\Lambda}^T$ has the following form:

$$\breve{\mathbf{\Sigma}} = \begin{pmatrix} \mathbf{V}_s & \mathbf{0} \\ \mathbf{0} & \mathbf{V}_p \end{pmatrix}, \tag{2}$$

where $\mathbf{V}_s$ is of size $K \times K$, $\mathbf{V}_p$ is of size $(p-K) \times (p-K)$ and K is a fixed number. The eigenvalues of $\mathbf{V}_s$ are $\breve{\alpha}_1 > \cdots > \breve{\alpha}_K > 0$ which are the K *spikes* of the ICV, and the eigen-

values of $\mathbf{V}_p$ are the *bulk* of the ICV. Naturally, it will be assumed that the spikes and the bulk do not overlap with each other. Such spiked spectrum of the ICV will generate a corresponding spiked structure for the PA-RCov $\mathcal{B}_m$, which is much in accordance with the reality.

The main task here is to infer the spiked eigenvalues of the ICV from those observed in the PA-RCov. This is achieved via the main theorem below which establishes a complex correspondence between the two sets of spikes. This result is established under two sets of assumptions. The first set of assumptions A1 - A8 follow the settings in Xia and Zheng (2014), that guarantee the consistency of the sequence $\mathcal{B}_m$. They are detailed in the supplementary material (Section B) with the proof of the theorem. The second set of assumptions B1 - B2 below are introduced to tackle the spiked structure of the ICV.

B1. $\breve{\mathbf{\Sigma}} = \mathbf{\Lambda}\mathbf{\Lambda}^T$ has the from in (2) where (i) $\mathbf{V}_s$ is of size $K \times K$ where K is a fixed number. The eigenvalues of $\mathbf{V}_s$ are $\breve{\alpha}_1 > \cdots > \breve{\alpha}_K > 0$. (ii) As $p \to \infty$, the ESD H_p of $\mathbf{V}_p$ converges in distribution to a nonrandom limiting distribution $\breve{H}$. (iii) The eigenvalues $\{\beta_{pj}\}$ of $\mathbf{V}_p$ are such that

$$\sup_j d(\beta_{pj}, \Gamma_{\breve{H}}) = \varepsilon_p \to 0,$$

where $d(x, A)$ denotes the distance of x to a set A and $\Gamma_{\breve{H}}$ is the support of $\breve{H}$.

B2. The sequence $(\breve{\mathbf{\Sigma}})_p$ is bounded in the spectral norm.

The main theoretical contribution of the paper is the following theorem which connects the spikes of $\mathcal{B}_m$ to those of the ICV. The proof of the theorem is given in the supplementary material (Section B).

Theorem 1. *Suppose that for all p, $(\mathbf{X}_t)$ is a p-dimensional process in Class $\mathcal{C}$ for some drift process $\boldsymbol{\mu}_t$ and co-volatility process $(\mathbf{\Theta}_t) = (\gamma_t \mathbf{\Lambda})$. Suppose also that Assumptions A1 - A8 and B1 - B2 hold. Define $\zeta = \int_0^1 (\gamma_t^*)^2 dt$, where γ_t^* is defined in Assumption A4, and*

$$\psi(\alpha) = \alpha + y \int \frac{t\alpha}{\alpha - t} dH(t), \tag{3}$$

where $H(x) = \breve{H}(x/\zeta)$ for all $x \geq 0$. Then, for a spiked eigenvalue α_j of the ICV satisfying

$$\psi'(\alpha_j) > 0,$$

there is an eigenvalue λ_j *of* $\mathcal{B}_m$ *such that*

$$\lambda_j \xrightarrow{a.s.} \psi(\alpha_j). \tag{4}$$

The main setting for Theorem 1 is close to that of Bai and Yao (2012) with however one major difference in the proof: Bai and Yao (2012) assume that samples are drawn from a purely multivariate normal distribution, while the stock returns also contain components from the finite variation process and the microstructure noise. As a result, these two parts should be dealt with before using the standard spiked model theory.

Therefore, according to Theorem 1, each spike α_j of the ICV will correspond to a spike λ_j of the PA-RCov, which tends to $\psi(\alpha_j)$. A natural estimator for α_j would be simply $\tilde{\alpha}_j = \psi^{-1}(\lambda_j)$. However, such direct inversion of the $\psi(\cdot)$ function suffers from many numerical instabilities. Following Bai and Ding (2012), a more stable estimator can be found using the following relationship

$$\alpha_j \underline{s}(\psi_j) = -1, \tag{5}$$

where $\psi_j = \psi(\alpha_j)$ and $\underline{s}(\cdot)$ denotes the companion Stieltjes transform of $F^{\mathcal{B}_\infty}$. For general information on Stieltjes transform and large sample covariance matrix, refer to Bai and Silverstein (2010). Indeed, Equation (5) is completely equivalent to (3). For details, please refer to Bai and Ding (2012). The advantage of (5) is that the Stieltjes transform $\underline{s}(\cdot)$ can be directly evaluated using the sample eigenvalues (λ_j) as follows. Let J be the set of indexes of α_j's. Then for each $z \notin \Gamma_{F^{\mathcal{B}_\infty}}$, we have

$$\underline{s}^*_m(z) = -\frac{1-p/m}{z} + \frac{1}{m}\sum_{k \notin J} \frac{1}{\lambda_k - z} \xrightarrow{a.s.} \underline{s}(z).$$

Therefore, since λ_j converging to $\psi(\alpha_j)$ by Theorem 1, define

$$b_{m,j} := -\frac{1-p/m}{\lambda_j} + \frac{1}{m}\sum_{k \notin J} \frac{1}{\lambda_k - \lambda_j}. \tag{6}$$

which provides a consistent estimator of $\underline{s}(\psi_j)$. Consequently, we have

$$-\frac{1}{b_{m,j}} \xrightarrow{a.s.} \alpha_j. \tag{7}$$

As a result, we define our estimator of the ICV spike α_j to be

$$\hat{\alpha}_j = -\frac{1}{b_{m,j}}$$

where $b_{m,j}$ is defined in (6). Theorem 1, or equivalently Equation (7) thus establishes the strong consistency of $\hat{\alpha}_j$. The proof of Theorem 1 is provided in the supplementary document.

3 Simulation studies

In this section, we check the finite-sample behavior of Theorem 1 by extensive simulations. We follow the procedure in Xia and Zheng (2014) to construct the simulated log-price process, which satisfies the assumptions we use. In particular, (γ_t) follows:

$$d\gamma_t = -\rho(\gamma_t - \mu_t)dt + \sigma d\tilde{W}_t, \quad \text{for } t \in [0,1],$$

where $\rho = 10$, $\sigma = 0.05$,

$$\mu_t = 2\sqrt{0.0009 + 0.0008\ \cos(2\pi t)},$$

and $\tilde{W}_t$ is a standard Brownian motion. A sample path of (γ_t) is given in Figure 2.

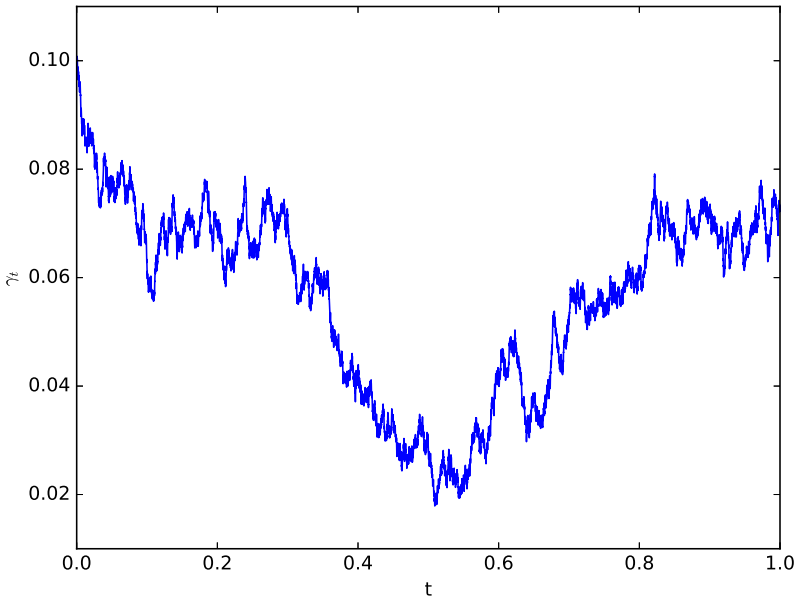

Figure 2: A sample path of the γ_t process

Additionally, the matrix $\breve{\boldsymbol{\Sigma}}$ is in the form of $\boldsymbol{UDU}^T$ where $\boldsymbol{U}$ is a randomly generated unitary matrix and $\boldsymbol{D}$ is a diagonal matrix. We set the first few diagonal entries as spikes and the rest of them are drawn independently from the Beta(1,3) distribution. For example, if there is one spike with a value of 2 for $\breve{\boldsymbol{\Sigma}}$, then the first diagonal entry of $\boldsymbol{D}$ is set to be 2 and the others are filled with independent Beta(1,3) samples. Then, the latent log price process $(\mathbf{X}_t)$ follows

$$d\mathbf{X}_t = \gamma_t \boldsymbol{\Lambda} d\mathbf{W}_t, \text{ where } \boldsymbol{\Lambda} = \breve{\boldsymbol{\Sigma}}^{1/2},$$

and $\mathbf{W}_t$ and $\tilde{W}_t$ are independent. Furthermore, the noise $(\boldsymbol{\varepsilon}_i)$ are drawn independently from $N(0, 0.0002\mathbf{I}_p)$. Under such structure, if we treat the largest eigenvalue of the integrated covariance matrix as the signal, then the mean noise-to-signal ratio, or the magnitude of the variation in the noise relative to the true signal, is 0.19% to 1.85%, depending on the choice of the spike. Such noise-to-signal ratio is similar to the reality, see Hansen and Lunde (2006) and Bandi and Russell (2008). Finally, we set $k = \lfloor 0.1n^{2/3} \rfloor$.

To illustrate the consistency, we fix the ratio $y = p/m$ to be 1, or 2. For each ratio, we set the asset dimension p to be 50, 100, 150, 200, 250 and 300, and use the equations $k = \lfloor 0.1n^{2/3} \rfloor$ and $m = \lfloor n/(2k) \rfloor$ to solve for the corresponding n. Then, the above simulation procedure is conducted and we get the pre-averaging estimator $\mathcal{B}_m$ by Equation (1). Using Equations (6) and (7), we get the estimator for the spikes (α_j) of the ICV. The true value for the spike of the ICV can be attained as follows. We use numerical method to estimate the integral $\int_0^1 \gamma_t^2 dt$ which is multiplied to the leading diagonal entries of the matrix $\boldsymbol{D}$ to produce a proxy of the true value for the spikes of the ICV. The whole procedure is repeated 500 times and the result is shown in Tables 1 to 4.

We consider four cases: one spike of magnitude 2, one spike of magnitude 5, two spikes of magnitude 3 and 1.5, respectively, and two spikes of magnitude 15 and 5, respectively. Note that these spikes are for $\breve{\boldsymbol{\Sigma}}$, not for the ICV. For each spike α_j, we report the empirical bias $|\hat{\alpha}_j - \alpha_j|$, its relative error $|\hat{\alpha}_j - \alpha_j|/|\alpha_j|$ measured in percentage, and the MSE of $\hat{\alpha}_j$. For the 2-spike case, the result in Tables 3 and 4 is separated by a comma where the result of the larger spike is before the comma and that of the smaller one is after the comma. For example, in Table 3 for two spikes 3 and 1.5, when $p = 100$ and $p/m = 1$, 0.0017(15.0) is for

the larger spike 3 and 0.0008(13.4) is for the smaller one 1.5. In addition, the percentage of error is shown inside the parentheses.

Table 1: Empirical bias, relative error (in %) and MSE of the spike estimates. Case 1: $K = 1$, $\alpha_1 = 2$.

	$p/m = 1$		$p/m = 2$	
	bias(%)	MSE	bias(%)	MSE
$p = 50$	0.0014(18.3)	0.0010	0.0018(23.1)	0.0012
$p = 100$	0.0010(12.7)	0.0007	0.0014(18.2)	0.0010
$p = 150$	0.0008(10.7)	0.0006	0.0012(15.2)	0.0008
$p = 200$	0.0007(9.6)	0.0006	0.0010(12.6)	0.0007
$p = 250$	0.0007(8.8)	0.0005	0.0010(12.4)	0.0007
$p = 300$	0.0006(7.6)	0.0004	0.0009(11.3)	0.0007

Table 2: Empirical bias, relative error (in %) and MSE of the spike estimates. Case 2: $K = 1$, $\alpha_1 = 5$.

	$p/m = 1$		$p/m = 2$	
	bias(%)	MSE	bias(%)	MSE
$p = 50$	0.0051(26.3)	0.0024	0.0057(29.4)	0.0031
$p = 100$	0.0038(19.8)	0.0019	0.0044(23.0)	0.0025
$p = 150$	0.0034(17.4)	0.0016	0.0038(19.7)	0.0022
$p = 200$	0.0029(15.3)	0.0015	0.0032(16.6)	0.0018
$p = 250$	0.0028(14.7)	0.0013	0.0031(15.9)	0.0018
$p = 300$	0.0025(13.1)	0.0013	0.0028(14.7)	0.0017

Table 3: Empirical bias, relative error (in %) and MSE of the spike estimates. Case 3: $K = 2$, $(\alpha_1, \alpha_2) = (3, 1.5)$.

	$p/m = 1$		$p/m = 2$	
	bias(%)	MSE	bias(%)	MSE
$p = 50$	0.0022(18.6), 0.0010(16.8)	0.0013, 0.0007	0.0025(21.5), 0.0012(20.4)	0.0016, 0.0009
$p = 100$	0.0017(15.0), 0.0008(13.4)	0.0011, 0.0006	0.0019(16.8), 0.0009(16.3)	0.0013, 0.0007
$p = 150$	0.0015(13.1), 0.0006(10.5)	0.0010, 0.0004	0.0017(14.3), 0.0008(13.7)	0.0012, 0.0006
$p = 200$	0.0013(11.0), 0.0005(9.1)	0.0008, 0.0004	0.0015(13.0), 0.0008(13.0)	0.0011, 0.0006
$p = 250$	0.0012(10.2), 0.0005(8.3)	0.0007, 0.0004	0.0013(11.6), 0.0006(11.0)	0.0010, 0.0006
$p = 300$	0.0011(9.4), 0.0005(7.9)	0.0007, 0.0003	0.0013(10.9), 0.0006(10.3)	0.0009, 0.0005

Table 4: Empirical bias, relative error (in %) and MSE of the spike estimates. Case 4: $K = 2$, $(\alpha_1, \alpha_2) = (15, 5)$.

	$p/m = 1$		$p/m = 2$	
	bias(%)	MSE	bias(%)	MSE
$p = 50$	0.0176(30.9), 0.0031(16.0)	0.0079, 0.0022	0.0181(31.2), 0.0046(23.7)	0.0095, 0.0033
$p = 100$	0.0167(28.8), 0.0029(14.8)	0.0056, 0.0018	0.0165(28.4), 0.0035(18.2)	0.0077, 0.0025
$p = 150$	0.0155(26.8), 0.0026(13.5)	0.0048, 0.0016	0.0155(26.7), 0.0031(16.1)	0.0065, 0.0020
$p = 200$	0.0137(23.7), 0.0026(13.2)	0.0046, 0.0014	0.0140(24.2), 0.0029(15.2)	0.0056, 0.0018
$p = 250$	0.0132(22.8), 0.0023(12.2)	0.0037, 0.0014	0.0133(22.9), 0.0028(14.7)	0.0056, 0.0018
$p = 300$	0.0125(21.6), 0.0022(11.6)	0.0035, 0.0012	0.0126(21.8), 0.0026(13.7)	0.0050, 0.0017

From Tables 1 to 4, we see that in general, the consistency holds quite well, that is, when the dimension p gets bigger, both the empirical bias and the MSE decrease in all situations. For instance, in Table 1 for $p/m = 1$, the mean percentage of error is reduced from 18.3% when $p = 50$, to only 7.6% for the case $p = 300$, achieving a quite satisfactory accuracy. In the meanwhile, this clear downward trend for errors for increasing p holds, in all four cases.

Generally, the error is smaller when $p/m = 1$ than that when $p/m = 2$. For example, when there are two spikes with values of 3 and 1.5, respectively, and $p = 300$, the errors are 9.4% and 7.9%, respectively for $p/m = 1$; they become 10.9% and 10.3%, respectively for $p/m = 2$. This phenomenon is quite reasonable and may be due to fact that we have more data points

to make inference for the value of spike when $p/m = 1$, given the same dimension p. However, it is found in general that the MSE for the estimation error is quite large, relative to the bias. This can be explained by the complexity of the simulation procedure used which involves continuous time diffusions and their discretization.

To conclude, the consistency of Theorem 1 for the spikes estimator is strongly confirmed by the extensive simulation studies, for various choices of spikes and their magnitudes, and different combinations of the pair of dimension and sample size.

4 Real data analysis

In order to compare our model with spikes (ModelSp) with that of Xia and Zheng (2014) without spikes (ModelWs), we apply the two models to the stocks in the US market and the Hong Kong market. We find that ModelSp not only appears to be a more natural choice from the empirical point of view, but also consistently provides more accurate estimation than ModelWs does. Here we present our main findings on the stocks in the US market. Analysis is also carried out for the stocks from the Hong Kong market which is presented in the Appendix A of the supplementary document.

Precisely, we analyze 92 stocks which are the available components of the S&P 100 index in the year 2008. The constituents of the S&P 100 index represent almost 45% of the market capitalization of the US equity market and most stocks stand for most established and largest companies in the US, which, in our point of view, are able to represent the US large-capitalization stocks. Among the 92 companies, 16 are in financial, 16 are in services, 14 are in basic materials, 13 are in healthcare, 12 are in technology, 10 are in industrial goods, 9 are in consumer goods and 2 are in utilities. The detailed list is provided in Section C of the supplementary document. We download the tick-by-tick data from the Wharton TAQ database. The sampling period starts from January 3rd, 2008 and ends at December 31st, 2008, totally 253 trading days. As usually done, only the transactions between 9:30 and 16:00 are considered. Moreover, the following cleaning procedures are adopted before constructing

the pre-averaging estimator. If there are multiple transactions in a single second, the median price for that second is retained. Here, we take the median of the prices for simplicity, and other methods may be used, for instance, randomly chosen price in the second, see Jing et al. (2016). For each second between 9:30 and 16:00, if there is no trade, the price of previous trade is taken as the price at that second. Therefore, we have 23401 prices for a stock in one day, the times 9:30 and 16:00 being included.

We then take the logarithm of these prices and construct the pre-averaging estimator $\mathcal{B}_m$ for every trading day, by setting $\theta = 0.19$ and $\alpha = 2/3$.

4.1 Detection of spikes and economic meaning of corresponding eigenvectors

To start with, we follow the approach in Passemier and Yao (2014) to estimate the number of spikes. The general idea is as follows. Consider the differences between consecutive eigenvalues of $\mathcal{B}_m$, $\lambda_1 \geq \lambda_2 \geq \cdots \geq \lambda_p$, as:

$$\delta_j := \lambda_j - \lambda_{j+1}, \quad j \geq 1.$$

Define a threshold d_m to be $Cm^{-2/3}\sqrt{2 \log \log m}$ where C is a tuning parameter which is data-driven. For the smallest j where $\delta_j < d_m$, the number of spikes of the ICV is estimated to be $\hat{K} = j - 1$. The tuning parameter C is set in the following way. The idea is to use the difference of the two largest eigenvalues of a random Wishart matrix, which corresponds to the case without any spikes. Five hundred independent replications are drawn to get an approximated distribution of the difference between the two largest eigenvalues for a random Wishart matrix. The tuning parameter C is taken to be

$$C = s \cdot m^{2/3}/\sqrt{2 \log \log m},$$

where the quantile s is estimated by the average of the 10th and the 11th largest spacings among these 500 replications. For details, please refer to Passemier and Yao (2014).

We find that there are several spikes for $\mathcal{B}_m$ almost everyday. The 253 numbers of spikes detected during the year 2008 are tabulated in Table 5.

Table 5: Distribution of the number of spikes $\hat{K}$ detected daily during 2008

$\hat{K}$	Count	Percent
1	38	15.02%
2	95	37.55%
3	84	33.20%
4	26	10.28%
5	9	3.56%
6	1	0.40%

We find that there are two or three spikes for most days, totally 70.75% of the whole year. A complete plot of these numbers is shown in Figure 5.

As an example, consider September 29th when the Dow index declines 777.68 points, the largest point drop in history. The corresponding spectrum of $\mathcal{B}_m$ is given in Figure 1. It is clearly seen that there is a spiked eigenvalue of $\mathcal{B}_m$ around 0.13, far larger than the rest of the eigenvalues, which confirms the spiked model we propose. Using the above detection method, we also find that $\hat{K} = 1$.

In addition, by analyzing the eigenvectors corresponding to the largest eigenvalues, we find that for the spiked eigenvalues, the eigenvectors do have some economic meanings. Almost all elements in the eigenvector corresponding to the largest eigenvalue share the same sign, which indicates that this eigenvector represents the market component. Moreover, we find the largest elements in the second eigenvector always represent those companies in the field of finance and basic materials, which indicates that the second eigenvector is a "vector of industry fields". However, eigenvectors corresponding to the "bulk" eigenvalues show no significant patterns and behave as random vectors. These findings confirm the conclusion drawn in Laloux et al. (2000) and Plerou et al. (2002). To illustrate, we take a look at the largest 10 elements in the eigenvector corresponding to the largest eigenvalue of $\mathcal{B}_m$ on September 29th:

Table 6: Largest ten components of the first eigenvector on September 29th, 2008

Stock	Firm	Industry
MS	Morgan Stanley	Financial
C	Citigroup Inc	Financial
BK	Bank of New York	Financial
BAC	Bank of America Corp	Financial
JPM	JP Morgan Chase & Co	Financial
GS	Goldman Sachs	Financial
AAPL	Apple Inc	Consumer goods
AIG	American International Group	Financial
USB	US Bancorp	Financial
AMZN	Amazon.com	Services

It is found from Table 6 that the first eigenvector consists of large companies from different industries, sharing the same sign, which reflects the market component. In the meantime, most companies are from the financial field, indicating also an industry signal. We also take a look at those companies corresponding to the largest values on the second to the fifth eigenvectors.

Table 7: Largest ten components of the second to fifth eigenvectors on September 29th, 2008

Stock	Firm	Industry	Stock	Firm	Industry
Second eigenvector			Third eigenvector		
AIG	American International Group	Financial	NOV	National Oilwell Varco	Basic materials
MA	Mastercard	Financial	AMZN	Amazon.com	Services
OXY	Occidental Petroleum Corp	Basic materials	APC	Anadarko Petroleum Corp	Basic materials
APC	Anadarko Petroleum Corp	Basic materials	DVN	Devon Energy	Basic materials
NOV	National Oilwell Varco	Basic materials	BLK	BlackRock Idec	Financial
MET	Metlife Inc	Financial	LOW	Lowe's	Services
GS	Goldman Sachs	Financial	QCOM	Qualcomm Inc	Technology
CAT	Caterpillar Inc	Industrial goods	EMR	Emerson Electric Co	Financial
APA	Apache Corp	Basic materials	HD	Home Depot	Services
GM	General Motors	Consumer goods	HAL	Halliburton	Basic materials
Fourth eigenvector			Fifth eigenvector		
BK	Bank of New York	Financial	MS	Morgan Stanley	Financial
QCOM	Qualcomm Inc	Technology	NOV	National Oilwell Varco	Basic materials
TWX	Time Warner Inc	Services	AMZN	Amazon.com	Services
EMC	EMC Corp	Technology	BLK	BlackRock Idec	Financial
ALL	Allstate Corp	Financial	APC	Anadarko Petroleum Corp	Basic materials
EXC	Exelon	Utilities	GS	Goldman Sachs	Financial
CMCSA	Comcast Corp	Services	APA	Apache Corp	Basic materials
GILD	Gilead Sciences	Healthcare	HAL	Halliburton	Basic materials
F	Ford Motor	Consumer goods	DVN	Devon Energy	Basic materials
T	AT%T Inc	Technology	COP	ConocoPhillips	Basic materials

No particular pattern is found in Table 7 and we think it is because these eigenvectors belong to the bulk eigenvalues.

4.2 The underlying relationship between the magnitude of spikes and the volatility of the S&P 100

Next, we consider the relationship between the spikes of $\mathcal{B}_m$ and the volatility of the S&P 100 index. We first plot the daily return of the S&P 100 index in the year 2008; and the volatility of the S&P 100 index (VXO) during the years 2008 and 2009, separated by the vertical line in the graph, in Figures 3 and 4, respectively.

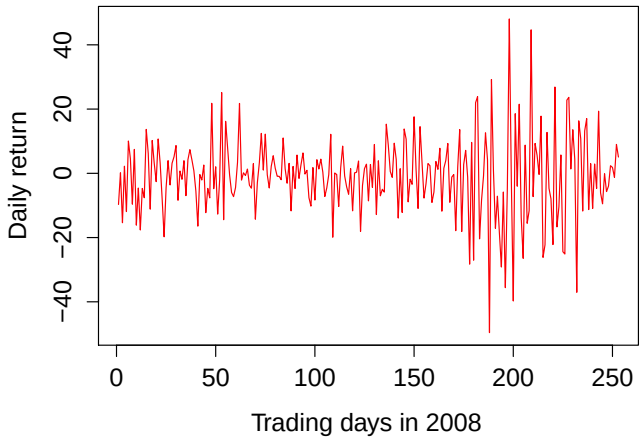

Figure 3: The daily return of the S&P 100 index during the year 2008

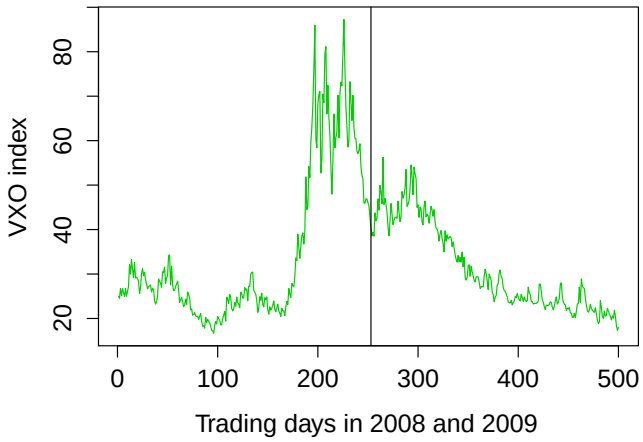

Figure 4: The VXO index during the years 2008 and 2009

From Figures 3 and 4, it is seen that during the first eight months (about 170 days) in the year 2008, the return and the volatility curves are relatively in peace. For example, the volatility fluctuates in the interval $[20, 30]$ during the period. However, starting from September 2008, the return series becomes volatile and the volatility reaches the peak during October to November, 2008. The VXO index reaches 80 during this period. After that, the volatility of the S&P 100 index starts going downward and this trend continues into the year

2009. We may also see the downtrend from the graph of the VXO index to the right of the middle line.

In addition, we plot the number of spikes for $\mathcal{B}_m$, and the magnitude of the largest eigenvalues for $\mathcal{B}_m$ during the year 2008, in Figures 5 and 6, respectively.

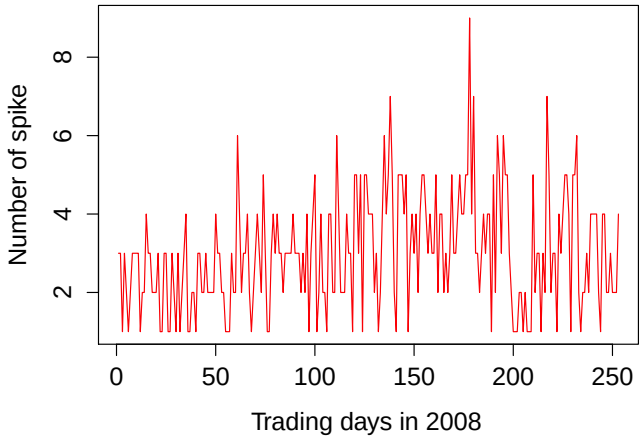

Figure 5: The number of spikes for $\mathcal{B}_m$ during the year 2008

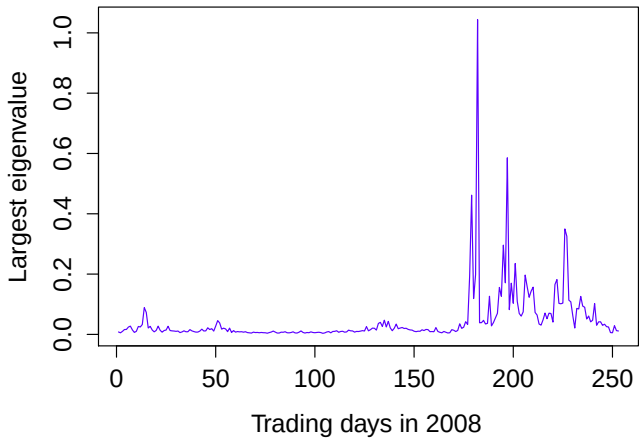

Figure 6: The largest eigenvalue of $\mathcal{B}_m$ during the year 2008

From Figure 6, we see that the oscillation starts from August, right before the peak of the

volatility of the S&P 100 index. Moreover, the relatively small values for the largest eigenvalue before and after the oscillation also appear before the stable situation for the volatility, that is, the small eigenvalues during January to July correspond to the small volatility during February to August; and small eigenvalues after November correspond to the volatility curve which gets smaller gradually starting from December, 2008. In addition, Figures 5 and 6 suggest that the peak for number of the spikes in the second part of the year seem coincident with that of the magnitude of eigenvalues. As a result, we conjecture that the magnitude of the largest eigenvalue may be a *leading indicator* of the volatility.

To confirm the above speculation, we calculate the cross correlation between the magnitude of the largest eigenvalue and the VXO index, which is shown in Figure 7. It is found that the most dominant cross correlations occur at lag -15, at about 0.57. In other words, the magnitude of the largest eigenvalue leads the VXO index for 15 trading days, or about three weeks. This is in agreement with the conjecture before, that the oscillation of the largest eigenvalue appears at the 182th trading day, about three weeks before the peak of the VXO at the 197th trading day.

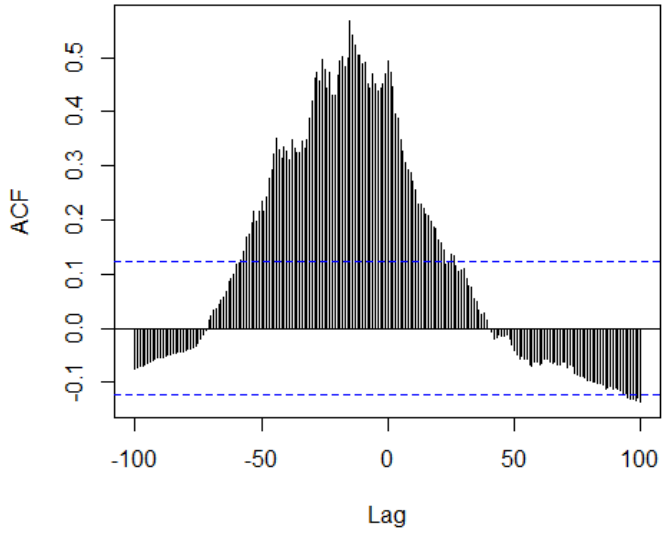

Figure 7: The cross correlation between the magnitude of the largest eigenvalue and the VXO index

In conclusion, our empirical findings described here suggest that the magnitude of the spikes

can be treated as a leading indicator of the volatility of the S&P 100 index. It makes sense since the largest eigenvalue always corresponds to the largest possible risk of the portfolio, which certainly reflects the possible volatility of the portfolio of the S&P 100 index.

4.3 Comparison of models with or without spikes

To compare ModelSp and ModelWs, we take two approaches, from empirical and statistical points of view, respectively. For every trading day, we use Equations (6) and (7) to estimate the spikes for ModelSp, and use the method in Xia and Zheng (2014) to estimate the bulk part of eigenvalues for both ModelSp and ModelWs. As said in the Introduction, their approach leads to a family of weights $(w_1, w_2, \cdots, w_N)$ on a grid of points $\{x_1 < x_2 < \cdots < x_N\}$.

(a) Qualitative comparison

To construct the ESD of the ICV using ModelSp, we first transform the spikes we detect into weights by assigning a weight of $1/p$ to each spike. Then, assuming there are M spikes detected, the largest k is found such that $\sum_{i=k}^{N} w_i > M/p$, and we set $w_k = \sum_{i=k}^{N} w_i - M/p$ and set $w_j = 0$, $j = k+1, \cdots, N$. Finally, we find the nearest grid point x_i for each spike and set the weight w_i to $1/p$. For each ESD, we plot a full version and magnified one for the spikes. For illustration, we randomly take September 29th and April 29th as examples, where one and three spikes are detected, respectively.

1. September 29th

We firstly take a look at the ESD of $\mathcal{B}_m$ in Figure 8. It is seen from the full version that most of the weights amass in the small range from 0 to 0.02. In addition, there is one large spike out of the bulk part, around 0.125.

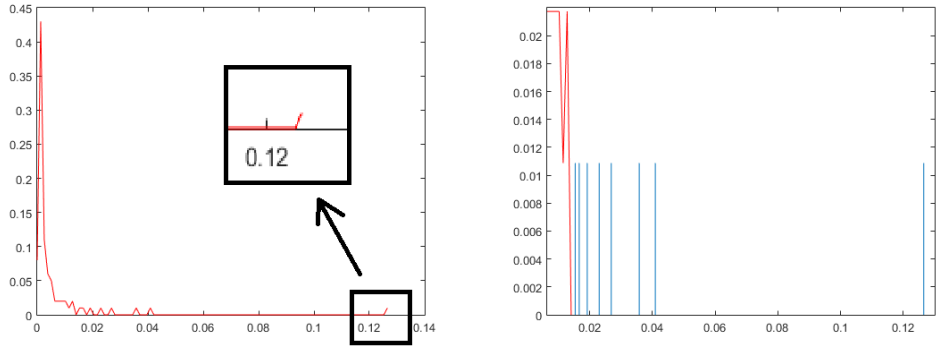

(a) Full version (b) Detailed version

Figure 8: The ESD of $\mathcal{B}_m$ on September 29th, 2008

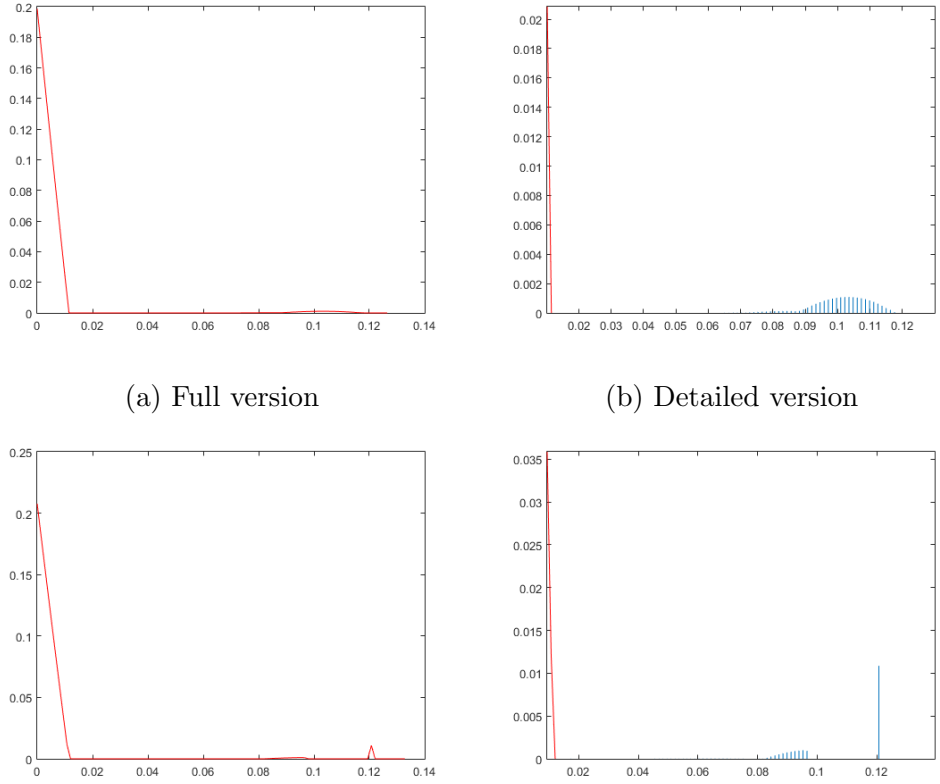

(a) Full version (b) Detailed version

(c) Full version (d) Detailed version

Figure 9: The ESD of the ICV estimated by ModelWs (top row) and by ModelSp (bottom row) on September 29th, 2008

For the ESD of the estimated ICV, we firstly look at top row in Figure 9 generated by Mod-

elWs. From Figure 9(a), we see that over 95% of weights concentrate in the small values ranging from 0 to 0.01. We also witness some really small weights around 0.1, compared with the bulk part. From Figure 9(b), it is seen that those grouped small weights indicate a continuous component, apart from the bulk.

For the ESD of the estimated ICV of ModelSp, the bottom row presents a totally different picture from that of ModelWs. There is one spike outside the bulk part and there are some negligibly small weights, compared with the spike. The "bulk + spikes" structure is clearly demonstrated here and is consistent with the ESD of $\mathcal{B}_m$, which is not shared by the ESD of the ICV generated by ModelWs.

2. April 29th

Next, we analyze the data on April 29th in Figures 10 and 11. We see that ModelSp catches the three spikes in the ESD of $\mathcal{B}_m$. In contrast, ModelWs produces a small smooth density in the range from 0.003 to 0.005, which we consider as a counterpart of the spike 0.0045 of $\mathcal{B}_m$. However, ModelWs is not able to detect other spikes, giving zero weight instead.

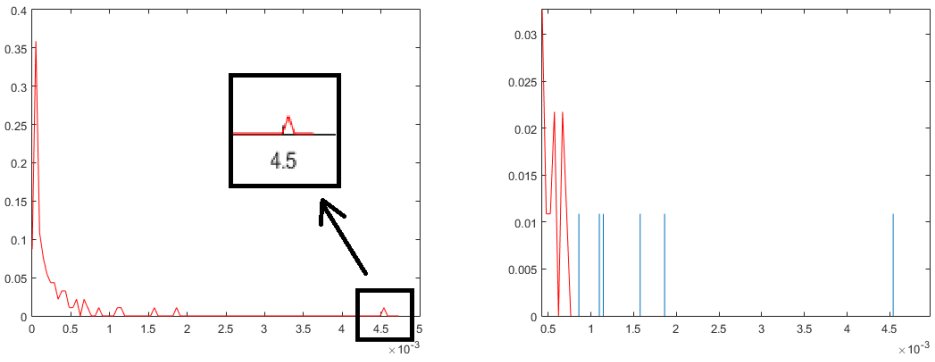

(a) Full version (b) Detailed version

Figure 10: The ESD of $\mathcal{B}_m$ on April 29th, 2008

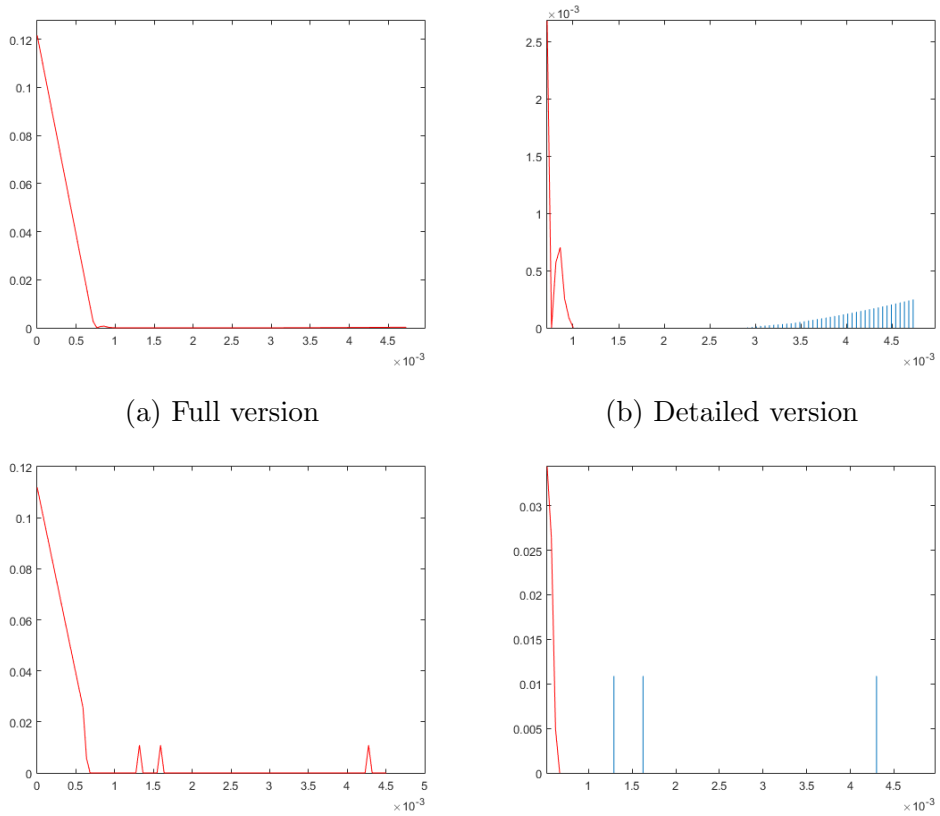

(a) Full version (b) Detailed version

(c) Full version (d) Detailed version

Figure 11: The ESD of the ICV estimated by ModelWs (top row) and by ModelSp (bottom row) on April 29th, 2008

In conclusion, ModelWs is able to detect the largest spike, which is estimated by a locally smooth continuous density around that spike. However, ModelWs frequently ignores weaker spikes, which are closer to the bulk part. On the other hand, ModelSp successfully detects all the spikes empirically seen in the spectrum of $\mathcal{B}_m$ so that the estimated spectrum by ModelSp clearly shows the "bulk + spikes" structure, which is consistent with that of $\mathcal{B}_m$.

(b) Quantitative comparison

In addition, we compare the two models from the statistical point of view. The idea is similar to a parametric bootstrap. Given the two ICV estimates by ModelWs and ModelSp, respectively, we generate by simulation the stock price processes, and obtain the corresponding PA-RCov matrices $\mathcal{B}_{m,Sp}$ and $\mathcal{B}_{m,Ws}$, for the two models, respectively. These simulated matrices are then compared to the observed PA-RCov $\mathcal{B}_m$. The smaller the difference is, the

better the model will be. Precisely, after getting the weight $(w_1, w_2, \cdots, w_N)$, we transform the weight on the grid into a set of estimated eigenvalues by the weight accumulation technique. We start with the smallest value of those points, x_1. We set $\lfloor w_1 \times p \rfloor$ eigenvalues to be x_1. Then, for the last x_i that we set to be eigenvalue, we find the smallest x_j such that $\lfloor (w_{i+1} + \cdots + w_j) \times p \rfloor > 0$, and set such number of eigenvalues to be x_j. The above procedure produces p eigenvalues for ModelWs given the weight $(w_1, w_2, \cdots, w_N)$. For ModelSp, we firstly do exactly the same thing as above to get p eigenvalues, and then replace the largest eigenvalues with those estimated from Equations (6) and (7), which also produces p eigenvalues. Note that only the largest few eigenvalues are different for the two models. We find that for the one spike case, there is only a slight difference between the two models. Moreover, for the case where there are two or more spikes, there is no big difference between the two models regarding the largest eigenvalue, which is below 10%. However, for other spikes, the difference between the two models is large, which is above 25%.

Since we do not know the true eigenvalues of the ICV, we compare the estimated ones as follows. As in Section 3, we generate the path for (γ_t) and evaluate the integral $\int_0^1 \gamma_t^2 dt$. As a result, we get the diagonal entries of the matrix D by dividing those eigenvalues we obtain above by this integral $\int_0^1 \gamma_t^2 dt$. Next, we follow the same procedure in the simulation to generate the log price process and calculate the pre-averaging estimator $\mathcal{B}_{m,Sp}$ and $\mathcal{B}_{m,Ws}$. Here, $p = 92$, $n = 23400$, $\theta = 0.19$ and $\alpha = 2/3$ in the simulation. Then, we compare the two matrices $\mathcal{B}_{m,Sp}$ and $\mathcal{B}_{m,Ws}$ with the original estimator $\mathcal{B}_m$.

We use both the spectral norm and the Frobenius norm to measure the distance between matrices. The simulation and comparison are conducted for the 253 days in 2008 and their averaged errors are shown in Table 8.

Table 8: Comparison of ModelWs and ModelSp regarding the simulation error

Model	Spectral norm	Frobenius norm
ModelWs	0.045	0.071
ModelSp	0.044	0.067

For the spectral norm, the two models perform nearly the same as ModelSp only provides

2.20% reduction of the error. For the Frobenius norm, ModelSp shows more improvement over the other model, reducing an average error of 4.22%. Since the only difference in the estimated eigenvalues of the two models is the spike part, small difference between the two models in Table 8 is expected. However, ModelSp shows better performance consistently. The smaller difference between the two models in term of the spectral norm can be explained by the fact that despite the absence of the explicit spiked structure, ModelWs is nevertheless capable to catch the largest eigenvalue. However, as explained previously, ModelWs is not able to estimate accurately the spikes other than the largest one. Meanwhile, the Frobenius distance takes into account all the eigenvalues. Therefore, the improvement by ModelSp over ModelWs becomes more significant in term of the Frobenius norm. This improvement is also amplified when more spikes exist in the spectrum of the ICV.

In conclusion, ModelSp has a theoretical support for the empirical "bulk + spikes" structure while ModelWs does not. Additionally, ModelSp outperforms ModelWs in the statistical analysis by generating more accurate pre-averaging realized covariance matrix in the tested situations. Finally, as mentioned earlier, analogous analysis has also been conducted for Hong Kong listed stocks. The conclusions are very close to the ones presented here for the US market. Details are to be found in Section A of the supplementary document.

5 Conclusions

Motivated by the "bulk + spikes" structure for the realized covariance matrix of multiple assets based on the noisy high-frequency data, and also the model in Xia and Zheng (2014) relating the limiting spectral distribution of the pre-averaging estimator and that of the ICV under the high-dimensional setup, we incorporate the spiked model into the spectrum estimation using high-frequency intraday data in the high-dimensional setting. Consistency of the estimated spikes is proved in the main theorem. Simulation studies demonstrate the finite-sample behavior of the consistency. It is found that for various choices of spikes and their magnitudes, and different combinations of the pair of dimension and sample size, the consistency holds quite satisfactorily.

In the real data analysis, we find that our model consistently outperforms that of Xia and Zheng (2014), from both empirical and statistical points of view. In addition, it is found that the magnitude of the largest spike is a potential leading indicator of the volatility of the portfolio which may be useful in practice.

Several possibilities exist to further our study. First, only the consistency is established for the estimator of the spikes. One can likely establish its asymptotic normality following the approach devised in Bai and Yao (2012). Second, for real financial application of the spike model, one may think about various kinds of option trading strategies which make use of the change of the spikes, for example, the stability of the largest spike for the realized covariance matrix is important for dispersion trading.

References

Andersen, T.G., Bollerslev, T., Diebold, F.X. and Labys, P. (2003). Modeling and Forecasting Realized Volatility. *Econometrica*, 71, 579-625.

Bai, Z., Chen, J. and Yao, J. (2010). On estimation of the population spectral distribution from a high-dimensional sample covariance matrix. *Australian & New Zealand Journal of Statistics*, 52(4), 423-437.

Bai, Z., and Ding, X. (2012). Estimation of spiked eigenvalues in spiked models. *Random Matrices: Theory and Applications*, 1(02), 1150011.

Bai, Z., and Silverstein, J. W. (2010). Spectral analysis of large dimensional random matrices. *New York: Springer*.

Bai, Z., and Yao, J. F. (2008). Central limit theorems for eigenvalues in a spiked population model. *In Annales de l'IHP Probabilits et statistiques*, 44(3), 447-474.

Bai, Z., and Yao, J. (2012). On sample eigenvalues in a generalized spiked population model. *Journal of Multivariate Analysis*, 106, 167-177.

Baik, J., and Silverstein, J. W. (2006). Eigenvalues of large sample covariance matrices of spiked population models. *Journal of Multivariate Analysis*, 97(6), 1382-1408.

Bandi, F.M. and Russell, J. R. (2008). Microstructure noise, realized variance, and optimal sampling. *The Review of Economic Studies*, 75(2), 339-369.

Barndorff-Nielsen, O.E., and Shephard, N. (2004). Econometric Analysis of Realized Covariation: High Frequency Based Covariance, Regression, and Correlation in Financial Economics. *Econometrica*, 72, 885-925.

Barndorff-Nielsen, O. E., Hansen, P. R., Lunde, A. and Shephard, N. (2008). Designing realized kernels to measure ex-post variation of equity prices in the presence of noise. *Econometrica*, 76, 1481-1536.

Barndorff-Nielsen, O. E., Hansen, P. R., Lunde, A. and Shephard, N. (2011). Multivariate realised kernels: consistent positive semi-definite estimators of the covariation of equity prices with noise and non-synchronous trading. *Journal of Econometrics*, 162(2), 149-169.

Christensen, K., Kinnebrock, S. and Podolskij, M. (2010). Pre-averaging estimators of the ex-post covariance matrix in noisy diffusion models with non-synchronous data. *Journal of Econometrics*, 159(1), 116-133.

Hansen, P.R. and Lunde, A. (2006). Realized variance and market microstructure noise. *Journal of Business and Economic Statistics*, 24, 127-161.

Jacod, J., Li, Y., Mykland, P. A., Podolskij, M. and Vetter, M. (2009). Microstructure noise in the continuous case: the pre-averaging approach. *Stochastic processes and their applications*, 119(7), 2249-2276.

Johnstone, I. M. (2001). On the distribution of the largest eigenvalue in principal components analysis. *Annals of statistics*, 295-327.

Jing, B.Y., Liu, Z. and Kong, X.B. (2016). Estimating volatility functionals with multiple transactions. *Econometric Theory*, 1-35.

Karoui, N. E. (2008). Spectrum estimation for large dimensional covariance matrices using random matrix theory. *Annals of Statistics*, 2757-2790.

Laloux, L., Cizeau, P., Potters, M. and Bouchaud, J. P. (2000). Random matrix theory and financial correlations. *International Journal of Theoretical and Applied Finance*, 3(3), 391-397.

Marcenko, V.A. and Pastur, L.A. (1967). Distribution of eigenvalues for some sets of random matrices. *Math. USSR-Sb*, 1, 457-483.

Mestre, X. (2008). Improved estimation of eigenvalues and eigenvectors of covariance matrices using their sample estimates. *Information Theory, IEEE Transactions on*, 54(11), 5113-5129.

Paul, D. (2007). Asymptotics of sample eigenstructure for a large dimensional spiked covariance model. *Statistica Sinica*, 1617-1642.

Passemier, D. and Yao, J. (2014). Estimation of the number of spikes, possibly equal, in the high-dimensional case. *Journal Of Multivariate Analysis*, 127, 173-183.

Plerou, V., Gopikrishnan, P., Rosenow, B., Amaral, L. A. N., Guhr, T. and Stanley, H. E. (2012). Random matrix approach to cross correlations in financial data. *Physical Review E*, 65(6), 066126.

Podolskij, M., Vetter, M., and Sommer, M. (2007). Estimation of volatility functionals in the simultaneous presence of microstructure noise and jumps. *Bernoulli*, 15, 634-658.

Silverstein, J. W., and Bai, Z. D. (1995). On the empirical distribution of eigenvalues of a class of large dimensional random matrices. *Journal of Multivariate analysis*, 54(2), 175-192.

Silverstein, J. W. and Choi, S. I. (1995). Analysis of the limiting spectral distribution of large-dimensional random matrices. *Journal of Multivariate analysis*, 54(2), 295-309.

Tao, T. (2012). Topics in random matrix theory. *Graduate Studies in Mathematics, vol. 132. American Mathematical Society, Providence, RI.*

Tao, M., Wang, Y., Yao, Y. and Zou, J. (2011). Large volatility matrix inference via combining low-frequency and high-frequency approaches. *Journal of American Statistical Association*, 106, 1025-1040.

Wang, Y., and Zou, J. (2010). Vast volatility matrix estimation for high-frequency financial data. *Annals of Statistics*, 38, 943-978.

Xia, N., and Zheng, X. (2014). On the inference about the spectra of high-dimensional covariance matrix based on high-frequency noisy observations. *arXiv: 1604.03638*.

Xiu, D. (2010). Quasi-maximum likelihood estimation of volatility with high frequency data. *Journal of Econometrics*, 159(1), 235-250.

Yao, J., Bai, Z., and Zheng, S. (2015). Large Sample Covariance Matrices and High-dimensional Data Analysis. *Cambridge University Press*.

Zhang, L., Mykland, P. A., and At-Sahalia, Y. (2005). A tale of two time scales. *Journal of American Statistical Association*, 100(472).

Zhang, L. (2011). Estimating covariation: Epps effect, microstructure noise. *Journal of Econometrics*, 160(1), 33-47.

Zheng, X., and Li, Y. (2011). On the estimation of integrated covariance matrices of high dimensional diffusion processes. *Annals of Statistics*, 39, 3121-3151.

Zheng, X., and Li, Y. (2011). Supplement to On the estimation of integrated covariance matrices of high dimensional diffusion processes..

arXiv:1702.03417v1 [stat.ME] 11 Feb 2017

Supplement to "On a spiked model for large volatility matrix estimation from noisy high-frequency data"

Keren Shen
Department of Statistics and Actuarial Science
The University of Hong Kong
Jianfeng Yao
Department of Statistics and Actuarial Science
The University of Hong Kong
and
Wai Keung Li
Department of Statistics and Actuarial Science
The University of Hong Kong

February 14, 2017

A The Hong Kong market

In this section, we compare the two models with the Hong Kong market, using the same technique in Section 4. We use 46 stocks which are the components of the Hang Seng index. Among these 46 stocks, 19 companies are from financial field, other companies are from conglomerates, services, consumer goods, utilities, basic materials and technology field. The whole list is available in the Appendix D. We download the tick-by-tick data from Bloomberg for transactions between 9:30 and 16:00, from September 1st, 2015 to March 10th, 2016, totally 127 trading days. The same cleaning procedures are implemented before constructing the pre-averaging estimator $\mathcal{B}_m$. We set $\theta = 0.19$ and $\alpha = 2/3$.

We use the same method in Section 4 to detect the number of spikes of Hong Kong data. The 127 numbers of spikes detected are tabulated in Table A1.

Table A1: Distribution of the number of spikes $\hat{K}$ detected daily

$\hat{K}$	Count	Percent
0	2	1.57%
1	70	55.12%
2	37	29.13%
3	17	13.39%
4	1	0.79%

It is seen that there are one or two spikes in most trading days, which are generally less than those for US stocks. One explanation is that there are fewer categories of companies in the Hong Kong market where 40% are from the financial field.

Then, we plot the daily returns of the Hang Seng index and the magnitude of the largest eigenvalue for each trading day, in Figures A1 and A2, respectively.

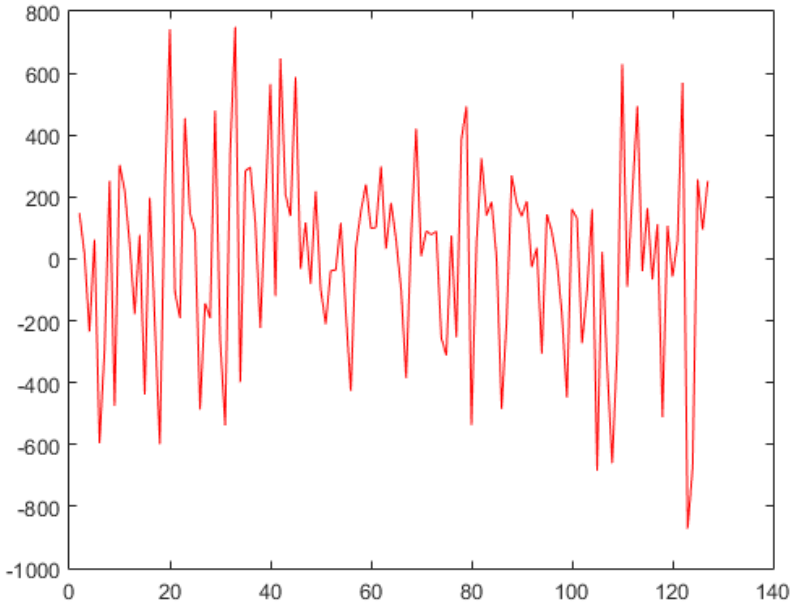

Figure A1: The daily return of the Hang Seng index

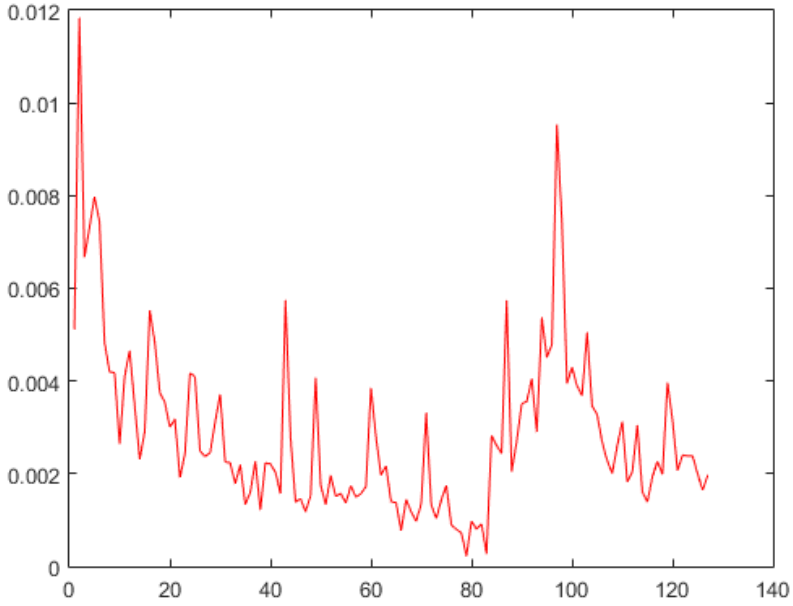

Figure A2: The largest eigenvalue of $\mathcal{B}_m$

From Figures A1 and A2, we see that the first large oscillation of the largest eigenvalue of $\mathcal{B}_m$ appears in the first ten days, right before the volatile movement of the Hang Seng index,

around the first twenty to forty days. Moreover, the second peak of the largest eigenvalue is around the one hundredth day, right before the second volatile oscillation of the daily return of the Hang Seng index, around 110th to 125th days. The findings are consistent with those for US stocks.

Moreover, the spectral distribution of $\mathcal{B}_m$ on November 11th, 2015 is plotted. It is seen from Figure A3 that the "bulk + spikes" structure is present for the Hong Kong market. There is one large spike valued 4×10^{-3}, away from the other eigenvalues. In addition, the largest ten components of the first to fourth eigenvectors on the same day are presented in Table A2.

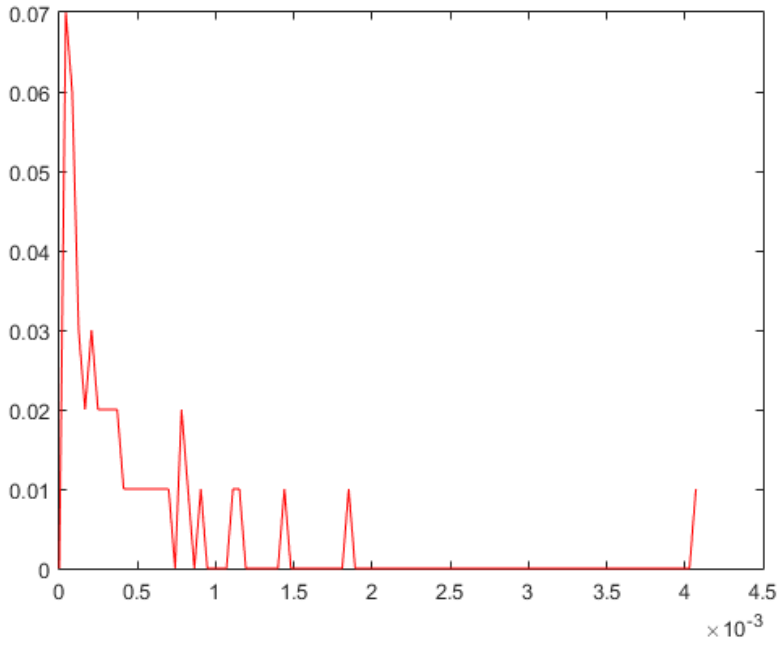

Figure A3: The ESD of $\mathcal{B}_m$ on November 11th, 2015

Table A2: Largest ten components of the first to fourth eigenvectors on November 11th, 2015

Stock	Firm	Industry	Stock	Firm	Industry
First eigenvector			Second eigenvector		
1088	China Shenhua	Basic materials	992	Lenovo	Technology
3328	BankComm	Financial	2319	Mengniu Dairy	Consumer goods
1299	AIA	Financial	1880	Belle Int'l	Consumer goods
2628	China Life	Financial	3988	Bank of China	Financial
1109	China Res Land	Financial	23	Bank of E Asia	Financial
883	CNOOC	Basic materials	762	China Unicom	Technology
12	Henderson Land	Financial	3	HK & China Gas	Utilities
857	PetroChina	Basic materials	688	China Overseas	Financial
992	Lenovo	Technology	16	SHK PPT	Financial
939	CCB	Financial	27	Galaxy Ent	Services
Third eigenvector			Fourth eigenvector		
322	TingYi	Consumer goods	2319	Mengniu Dairy	Consumer goods
992	Lenovo	Technology	151	Want Want China	Consumer goods
135	Kunlun Energy	Basic materials	1109	China Res Land	Financial
83	Sino Land	Financial	2388	BOC Hong Kong	Financial
151	Want Want China	Consumer goods	144	China Mer Hold	Services
2388	BOC Hong Kong	Financial	823	Link Reit	Financial
4	Wharf Holdings	Financial	494	Li & Fung	Services
1880	Bell Int'l	Consumer goods	11	Hang Seng Bank	Financial
823	Link Reit	Financial	23	Bank of E Asia	Financial
267	CITIC	Basic materials	1044	Hengan Int'l	Consumer goods

All but one elements in the first eigenvector share the same sign, indicating the first eigenvector represents a market component. The other eigenvectors show no particular patterns, which include all kinds of stocks from different fields. From eigenvectors, we may conclude that we have one interpretable spike.

We use the same statistical approach as in Section 4 to compare ModelSp with ModelWs. The weight accumulating procedure generates the same phenomenon of two groups of eigenvalues as that for the US stocks. There is no big difference between the largest eigenvalues of the two models while the difference is larger for other spikes. The result of the statistical comparison is shown in Table A3.

Table A3: Comparison of ModelWs and ModelSp regarding the simulation error

Model	Spectral norm	Frobenius norm
ModelWs	0.0036	0.0079
ModelSp	0.0035	0.0078

For the spectral norm, ModelSp produces an average error which is 3.15% less than that of ModelWs. For the Frobenius norm, the error produced by ModelSp is 2.83% less than that of ModelWs. In a word, ModelSp shows some improvement over ModelWs.

All in all, the same conclusion can be drawn from the Hong Kong data as in the US market that ModelSp shows superior performance over ModelWs, both empirically and statistically.

B Proof of Theorem 1

We first set some notations that will be used throughout the proof. For any real matrix $\mathbf{B}$, $\|\mathbf{B}\| = \sqrt{\lambda_{\max}(\mathbf{B}\mathbf{B}^T)}$ denotes its spectral norm, where $\lambda_{\max}$ denotes the largest eigenvalue. Moreover, $\mathbf{B}_i$ denotes the ith column of $\mathbf{B}$ and b_i^j denotes the jth entry in $\mathbf{B}_i$. For any nonnegative definite matrix $\mathbf{B}$, $\mathbf{B}^{1/2}$ denotes a Hermitian square root. For any vector $\mathbf{x}$, $|\mathbf{x}|$ stands for its Euclidean norm and x^j denotes its jth entry. Additionally, "$\stackrel{d}{=}$" means equal in distribution, $Y_n = O_p(f(n))$ means that the sequence $(|Y_n|/f(n))$ is tight, and $Y_n = o_p(f(n))$ means that $Y_n/f(n) \xrightarrow{p} 0$.

Next, we detail below the set of assumptions A1-A8 borrowed from Xia and Zheng (2014). Note that the only difference is that in A3 we let (γ_t) and $(\mathbf{W}_t)$ be independent, for simplicity.

A1. For all p, $(\mathbf{X}_t)$ is a p-dimensional process for some drift process $\boldsymbol{\mu}_t = (\mu_t^1, \cdots, \mu_t^p)^T$ and co-volatility process $(\boldsymbol{\Theta}_t)$. Moreover, almost surely, there exist $(\gamma_t) \in D([0,1];\mathbb{R})$ and $\boldsymbol{\Lambda}$ a $p \times p$ matrix satisfying $\mathrm{tr}(\boldsymbol{\Lambda}\boldsymbol{\Lambda}^T) = p$ such that

$$\boldsymbol{\Theta}_t = \gamma_t \boldsymbol{\Lambda},$$

where $D([0,1];\mathbb{R})$ is the space of càdlàg functions from $[0,1]$ to $\mathbb{R}$.

A2. There exists a $C_0 < \infty$ such that for all p and all $j = 1, \cdots, p$, $|\mu_t^j| \leq C_0$ for all $t \in [0, 1)$ almost surely.

A3. (γ_t) and $(\mathbf{W}_t)$ are independent for all $t \in [0, 1)$.

A4. There exists a $C_1 < \infty$ such that for all p, $|\gamma_t| \in (1/C_1, C_1)$ for all $t \in [0, 1)$ almost surely, and in addition, almost surely, (γ_t) converges uniformly to a nonzero process (γ_t^*) that is piecewise continuous with finitely many jumps when $p \to \infty$.

A5. There exists a $C_2 < \infty$ such that for all p and all $j = 1, \cdots, p$, the individual volatilities $\sigma_{j,t} = \sqrt{(\gamma_t)^2 \cdot \sum_{k=1}^{p} (\Lambda_{jk})^2} \in (1/C_2, C_2)$ for $t \in [0, 1)$ almost surely, where $\Lambda = (\Lambda_{jk})$.

A6. For all $j = 1, \cdots, p$, the noise (ε_i^j) is stationary with mean 0 and bounded 4ℓth moments and with ρ-mixing coefficients $\rho^j(r)$ satisfying
$\max_{j=1,\cdots,p} \rho^j(r) = O(r^{-\ell})$ for some integer $\ell \geq 2$ as $r \to \infty$.

A7. There exists a $C_3 < \infty$ and $0 \leq \delta < 1/2$ such that for all p, $\|\text{ICV}\| \leq C_3 p^\delta$ almost surely.

A8. $k = \lfloor \theta n^\alpha \rfloor$ for some $\theta \in (0, \infty)$ and $\alpha \in [\alpha_0, 1)$, and $m = \lfloor n/(2k) \rfloor$ satisfying that $\lim_{p \to \infty} p/m = y > 0$, where $\alpha_0 = \max\{(3 + \ell)/(2\ell + 2), 2/3\}$ and ℓ is the integer in Assumption A6.

Before the proof for Theorem 1, we establish two lemmas.

Lemma 1. *Let*

$$\tilde{\mathbf{V}}_i = \sum_{|j|<k} (1 - \frac{|j|}{k}) \int_{\frac{(2i-1)k+j-1}{n}}^{\frac{(2i-1)k+j}{n}} \boldsymbol{\mu}_t dt = (\breve{v}_i^1, \cdots, \breve{v}_i^p)^T,$$

$$w_i = \sum_{|j|<k} (1 - \frac{|j|}{k})^2 \int_{\frac{(2i-1)k+j-1}{n}}^{\frac{(2i-1)k+j}{n}} \gamma_t^2 dt,$$

and

$$\Delta\bar{\boldsymbol{\varepsilon}}_{2i} = (\Delta\bar{\varepsilon}_{2i}^1, \cdots, \Delta\bar{\varepsilon}_{2i}^p)^T.$$

Then, $\breve{v}_i^j = O_p(k/n)$, $w_i = O_p(k/n)$. *Moreover,* $\Delta\bar{\varepsilon}_{2i}^j = O_p(1/\sqrt{k})$ *for any* $i = 1, \cdots, m$ *and all* $j = 1, \cdots, p$.

Proof. For any process $\mathbf{V} = (\mathbf{V}_t)_{t\geq 0}$, let

$$\Delta \mathbf{V}_i = \mathbf{V}_{i/n} - \mathbf{V}_{(i-1)/n}, \bar{\mathbf{V}}_i = \frac{1}{k}\sum_{j=0}^{k-1} \mathbf{V}_{((i-1)k+j)/n}, \text{ and } \Delta\bar{\mathbf{V}}_{2i} = \bar{\mathbf{V}}_{2i} - \bar{\mathbf{V}}_{2i-1}.$$

Note that $\Delta\bar{\mathbf{V}}_{2i}$ can be written as

$$\begin{aligned}
\Delta\bar{\mathbf{V}}_{2i} &= \frac{1}{k}\sum_{j=0}^{k-1}(\mathbf{V}_{((2i-1)k+j)/n} - \mathbf{V}_{((2i-2)k+j)/n}) \\
&= \frac{1}{k}\sum_{j=0}^{k-1}\sum_{\ell=1}^{k} \Delta\mathbf{V}_{(2i-2)k+j+\ell} \\
&= \sum_{|j|<k}(1-\frac{|j|}{k})\Delta\mathbf{V}_{(2i-2)k+j}.
\end{aligned}$$

The result is then easily proved by Assumptions A2, A4, and A6. □

Lemma 2. *Let* $\breve{\mathbf{\Sigma}}^{1/2}\mathbf{Z} := (\breve{Z}^1, \cdots, \breve{Z}^p)^T$*, where* $\mathbf{Z}$ *is a p-dimensional vector consisting of i.i.d standard normal random variables. Then,* $\breve{Z}^j = O_p(1)$ *for all* $j = 1, \cdots, p$*.*

Proof. Let $\breve{Z}^j = \sum_{k=1}^p \lambda_k^j Z^k$, where Z^k's are i.i.d standard normal distributed variates. Therefore, from Assumption A5,

$$\breve{Z}^j = \sum_{k=1}^{p} \lambda_k^j Z^k \overset{d}{=} N(0, \sum_{k=1}^{p}(\lambda_k^j)^2) = O_p(1)$$

for all p and j. □

Proof of Theorem 1. We have

$$\begin{aligned}
\Delta\bar{\mathbf{Y}}_{2i} &= \Delta\bar{\mathbf{X}}_{2i} + \Delta\bar{\boldsymbol{\varepsilon}}_{2i} \\
&= \tilde{\mathbf{V}}_i + \sqrt{w_i}\breve{\mathbf{\Sigma}}^{1/2}\mathbf{Z}_i + \Delta\bar{\boldsymbol{\varepsilon}}_{2i},
\end{aligned}$$

where

$$\tilde{\mathbf{V}}_i = \sum_{|j|<k}(1-\frac{|j|}{k})\int_{\frac{(2i-1)k+j-1}{n}}^{\frac{(2i-1)k+j}{n}} \boldsymbol{\mu}_t dt,$$

$$w_i = \sum_{|j|<k}(1-\frac{|j|}{k})^2\int_{\frac{(2i-1)k+j-1}{n}}^{\frac{(2i-1)k+j}{n}} \gamma_t^2 dt,$$

and $\mathbf{Z}_i = (Z_i^1, \cdots, Z_i^p)^T$ consists of independent standard normal random variates. As a result,

$$\begin{aligned}
\tilde{\mathbf{\Sigma}} &= \frac{p}{m}\sum_{i=1}^{m}\frac{\Delta\bar{\mathbf{Y}}_{2i}(\Delta\bar{\mathbf{Y}}_{2i})^T}{|\Delta\bar{\mathbf{Y}}_{2i}|^2} \\
&= \frac{p}{m}\sum_{i=1}^{m}\frac{(\tilde{\mathbf{V}}_i + \sqrt{w_i}\breve{\mathbf{\Sigma}}^{1/2}\mathbf{Z}_i + \Delta\bar{\boldsymbol{\varepsilon}}_{2i})(\tilde{\mathbf{V}}_i + \sqrt{w_i}\breve{\mathbf{\Sigma}}^{1/2}\mathbf{Z}_i + \Delta\bar{\boldsymbol{\varepsilon}}_{2i})^T}{|\tilde{\mathbf{V}}_i + \sqrt{w_i}\breve{\mathbf{\Sigma}}^{1/2}\mathbf{Z}_i + \Delta\bar{\boldsymbol{\varepsilon}}_{2i}|^2} \\
&= \frac{p}{m}\sum_{i=1}^{m}\frac{(\frac{\tilde{\mathbf{V}}_i+\Delta\bar{\boldsymbol{\varepsilon}}_{2i}}{\sqrt{w_i}} + \breve{\mathbf{\Sigma}}^{1/2}\mathbf{Z}_i)(\frac{\tilde{\mathbf{V}}_i+\Delta\bar{\boldsymbol{\varepsilon}}_{2i}}{\sqrt{w_i}} + \breve{\mathbf{\Sigma}}^{1/2}\mathbf{Z}_i)^T}{|\frac{\tilde{\mathbf{V}}_i+\Delta\bar{\boldsymbol{\varepsilon}}_{2i}}{\sqrt{w_i}} + \breve{\mathbf{\Sigma}}^{1/2}\mathbf{Z}_i|^2} \\
&= \frac{p}{m}\sum_{i=1}^{m}\frac{(\mathbf{V}_i + \breve{\mathbf{\Sigma}}^{1/2}\mathbf{Z}_i)(\mathbf{V}_i + \breve{\mathbf{\Sigma}}^{1/2}\mathbf{Z}_i)^T}{|\mathbf{V}_i + \breve{\mathbf{\Sigma}}^{1/2}\mathbf{Z}_i|^2},
\end{aligned}$$

where $\mathbf{V}_i = (\tilde{\mathbf{V}}_i + \Delta\bar{\boldsymbol{\varepsilon}}_{2i})/\sqrt{w_i}$. From Lemma 1, we know that $\tilde{v}_i^j = O(k/n)$, $\Delta\bar{\boldsymbol{\varepsilon}}_{2i}^j = O_p(1/\sqrt{k})$, and $w_i = O_p(k/n)$, for all i and j. Therefore, from Assumption A8,

$$v_i^j = O_p(\sqrt{k/n}) = O_p(1/\sqrt{p}), \tag{A1}$$

so that $|\mathbf{V}_i|$ are uniformly bounded.

We borrow the following convergence result proved in Xia and Zheng (2014):

$$\max_{i=1,\cdots,m}||\breve{\mathbf{\Sigma}}^{1/2}\mathbf{Z}_i|^2/p - 1| = \max_{i=1,\cdots,m}|\mathbf{Z}_i^T\breve{\mathbf{\Sigma}}\mathbf{Z}_i/p - 1| \to 0, \text{ almost surely.}$$

Consequently, we have

$$\max_{i=1,\cdots,m}||\mathbf{V}_i + \breve{\mathbf{\Sigma}}^{1/2}\mathbf{Z}_i|^2/p - 1| \to 0, \quad \text{almost surely.}$$

In other words, we may focus on

$$\begin{aligned}
\mathbf{S}_m &= \frac{1}{m}\sum_{i=1}^{m}(\mathbf{V}_i + \breve{\mathbf{\Sigma}}^{1/2}\mathbf{Z}_i)(\mathbf{V}_i + \breve{\mathbf{\Sigma}}^{1/2}\mathbf{Z}_i)^T \\
&= \frac{1}{m}\sum_{i=1}^{m}(\mathbf{V}_i + \mathbf{W}_i)(\mathbf{V}_i + \mathbf{W}_i)^T,
\end{aligned}$$

where we let $\mathbf{W}_i := \breve{\mathbf{\Sigma}}^{1/2}\mathbf{Z}_i$.

We have

$$\breve{\mathbf{\Sigma}} = \begin{pmatrix} \mathbf{V}_s & \mathbf{0} \\ \mathbf{0} & \mathbf{V}_p \end{pmatrix},$$

where $\mathbf{V}_s$ is of size $K \times K$ and $\mathbf{V}_p$ is of size $(p-K) \times (p-K)$. Similar to the approach of Yao et al. (2015), decompose the p-dimensional vectors $\mathbf{V}_i$, $\mathbf{W}_i$ and $\mathbf{Z}_i$ into blocks of size K and $p-K$, respectively:

$$\mathbf{V}_i = \begin{pmatrix} \mathbf{V}_{1i} \\ \mathbf{V}_{2i} \end{pmatrix}, \quad \mathbf{W}_i = \begin{pmatrix} \mathbf{W}_{1i} \\ \mathbf{W}_{2i} \end{pmatrix}, \quad \mathbf{Z}_i = \begin{pmatrix} \mathbf{Z}_{1i} \\ \mathbf{Z}_{2i} \end{pmatrix}.$$

Then, we may write

$$\begin{aligned} \mathbf{S}_m &= \frac{1}{m}\sum_{i=1}^{m}(\mathbf{V}_i + \mathbf{W}_i)(\mathbf{V}_i + \mathbf{W}_i)^T \\ &= \frac{1}{m}\begin{pmatrix} (\mathbf{V}_{(1)} + \mathbf{W}_{(1)})(\mathbf{V}_{(1)} + \mathbf{W}_{(1)})^T & (\mathbf{V}_{(1)} + \mathbf{W}_{(1)})(\mathbf{V}_{(2)} + \mathbf{W}_{(2)})^T \\ (\mathbf{V}_{(2)} + \mathbf{W}_{(2)})(\mathbf{V}_{(1)} + \mathbf{W}_{(1)})^T & (\mathbf{V}_{(2)} + \mathbf{W}_{(2)})(\mathbf{V}_{(2)} + \mathbf{W}_{(2)})^T \end{pmatrix} \\ &:= \begin{pmatrix} \mathbf{S}_{11} & \mathbf{S}_{12} \\ \mathbf{S}_{21} & \mathbf{S}_{22} \end{pmatrix}, \end{aligned}$$

where

$$\mathbf{V}_{(1)} = (\mathbf{V}_{11}, \cdots, \mathbf{V}_{1m}), \quad \mathbf{V}_{(2)} = (\mathbf{V}_{21}, \cdots, \mathbf{V}_{2m}),$$

and

$$\mathbf{W}_{(1)} = (\mathbf{W}_{11}, \cdots, \mathbf{W}_{1m}), \quad \mathbf{W}_{(2)} = (\mathbf{W}_{21}, \cdots, \mathbf{W}_{2m}).$$

Similarly, define the analogous decomposition for $\mathbf{Z}_i$ vectors to form $\mathbf{Z}_{(1)}$ and $\mathbf{Z}_{(2)}$ such that

$$\mathbf{W}_{(1)} = \mathbf{V}_s^{1/2}\mathbf{Z}_{(1)}, \quad \mathbf{W}_{(2)} = \mathbf{V}_p^{1/2}\mathbf{Z}_{(2)}.$$

An eigenvalue λ_i of $\mathbf{S}_m$ that is not an eigenvalue of $\mathbf{S}_{22}$ satisfies

$$0 = |\lambda_i \mathbf{I}_p - \mathbf{S}_m| = |\lambda_i \mathbf{I}_{p-K} - \mathbf{S}_{22}| \cdot |\lambda_i \mathbf{I}_K - \mathbf{K}_m(\lambda_i)|,$$

where

$$\mathbf{K}_m(\ell) = \mathbf{S}_{11} + \mathbf{S}_{12}(\ell \mathbf{I}_{p-K} - \mathbf{S}_{22})^{-1}\mathbf{S}_{21}.$$

This will happen if λ_i tends to a location outside the support of the limiting spectral distribution (LSD) of $\mathbf{S}_m$ (the same as the LSD of $\mathbf{S}_{22}$) so that for such λ_i and large m, it will hold that $|\lambda_i \mathbf{I}_{p-K} - \mathbf{S}_{22}| \neq 0$, so that necessarily

$$|\lambda_i \mathbf{I}_K - \mathbf{K}_m(\lambda_i)| = 0.$$

Consider a real number ℓ outside the support of the LSD of $\mathbf{S}_{22}$, it holds that

$$\begin{aligned}
\mathbf{K}_m(\ell) &= \mathbf{S}_{11} + \mathbf{S}_{12}(\ell\mathbf{I}_{p-K} - \mathbf{S}_{22})^{-1}\mathbf{S}_{21} \\
&= \frac{1}{m}(\mathbf{V}_{(1)} + \mathbf{W}_{(1)})\{\mathbf{I}_m + \frac{1}{m}(\mathbf{V}_{(2)} + \mathbf{W}_{(2)})^T(\ell\mathbf{I}_{p-K} - \frac{1}{m}(\mathbf{V}_{(2)} + \mathbf{W}_{(2)})(\mathbf{V}_{(2)} + \mathbf{W}_{(2)})^T)^{-1} \\
&\quad (\mathbf{V}_{(2)} + \mathbf{W}_{(2)})\}(\mathbf{V}_{(1)} + \mathbf{W}_{(1)})^T \\
&= \frac{\ell}{m}(\mathbf{V}_{(1)} + \mathbf{W}_{(1)})(\ell\mathbf{I}_m - \frac{1}{m}(\mathbf{V}_{(2)} + \mathbf{W}_{(2)})^T(\mathbf{V}_{(2)} + \mathbf{W}_{(2)}))^{-1}(\mathbf{V}_{(1)} + \mathbf{W}_{(1)})^T \\
&= \frac{\ell}{m}(\mathbf{V}_{(1)} + \mathbf{V}_s^{1/2}\mathbf{Z}_{(1)})(\ell\mathbf{I}_m - \frac{1}{m}(\mathbf{V}_{(2)} + \mathbf{W}_{(2)})^T(\mathbf{V}_{(2)} + \mathbf{W}_{(2)}))^{-1}(\mathbf{V}_{(1)}^T + \mathbf{Z}_{(1)}^T\mathbf{V}_s^{1/2}),
\end{aligned}$$

where the third equality uses the following identity: for $\ell \neq 0$ which is not an eigenvalue of $\mathbf{A}^T\mathbf{A}$,

$$\mathbf{I}_m + \mathbf{A}(\ell\mathbf{I}_{p-K} - \mathbf{A}^T\mathbf{A})^{-1}\mathbf{A}^T \equiv \ell(\ell\mathbf{I}_m - \mathbf{A}\mathbf{A}^T)^{-1}.$$

Since ℓ is outside the support of the LSD of $\mathbf{S}_{22}$, for large m, the norm of $(\ell\mathbf{I}_m - \frac{1}{m}(\mathbf{V}_{(2)} + \mathbf{W}_{(2)})^T(\mathbf{V}_{(2)} + \mathbf{W}_{(2)}))^{-1}$ is bounded. Therefore,

$$\begin{aligned}
& \|\frac{\ell}{m}\mathbf{V}_{(1)}(\ell\mathbf{I}_m - \frac{1}{m}(\mathbf{V}_{(2)} + \mathbf{W}_{(2)})^T(\mathbf{V}_{(2)} + \mathbf{W}_{(2)}))^{-1}\mathbf{V}_{(1)}^T\| \\
\leq\ & \frac{\ell}{m}\|\mathbf{V}_{(1)}\|^2\|(\ell\mathbf{I}_m - \frac{1}{m}(\mathbf{V}_{(2)} + \mathbf{W}_{(2)})^T(\mathbf{V}_{(2)} + \mathbf{W}_{(2)}))^{-1}\| \\
=\ & \frac{C}{m}\|\mathbf{V}_{(1)}\mathbf{V}_{(1)}^T\| \\
\leq\ & \frac{C}{m}\mathrm{tr}(\mathbf{V}_{(1)}\mathbf{V}_{(1)}^T) \\
=\ & \frac{C}{m}\sum_{i=1}^{m}\sum_{j=1}^{K}(v_i^j)^2 \\
=\ & O_p(\frac{1}{p}) = o_p(1),
\end{aligned}$$

as $\max_{i=1,\cdots,m} v_i^j = O_p(1/\sqrt{p})$ for all p and all j, from Equation (A1). From Lemma 2, we know that the order of the magnitude of the elements in $\mathbf{Z}_{(1)}^T\mathbf{V}_s^{1/2}$ is $O_p(1)$ so that similarly we have

$$\begin{aligned}
& \|\frac{\ell}{m}\mathbf{V}_{(1)}(\ell\mathbf{I}_m - \frac{1}{m}(\mathbf{V}_{(2)} + \mathbf{W}_{(2)})^T(\mathbf{V}_{(2)} + \mathbf{W}_{(2)}))^{-1}\mathbf{Z}_{(1)}^T\mathbf{V}_s^{1/2}\| \\
\leq\ & \frac{\ell}{m}\|\mathbf{V}_{(1)}\|\|(\ell\mathbf{I}_m - \frac{1}{m}(\mathbf{V}_{(2)} + \mathbf{W}_{(2)})^T(\mathbf{V}_{(2)} + \mathbf{W}_{(2)}))^{-1}\|\|\mathbf{Z}_{(1)}^T\mathbf{V}_s^{1/2}\| \\
\leq\ & \frac{C}{m}\sqrt{m} = O_p(\frac{1}{\sqrt{p}}) = o_p(1).
\end{aligned}$$

Therefore, by the Law of Large Numbers,

$$\begin{aligned}\mathbf{K}_m(\ell) &= \mathbf{V}_s \cdot [\ell \cdot \mathrm{tr}(\ell \mathbf{I}_m - \frac{1}{m}(\mathbf{V}_{(2)} + \mathbf{W}_{(2)})^T(\mathbf{V}_{(2)} + \mathbf{W}_{(2)}))^{-1}/m] + o_{a.s.}(1) \\ &= -\mathbf{V}_s \cdot \ell \breve{\underline{s}}(\ell) + o_{a.s.}(1),\end{aligned}$$

where $\breve{\underline{s}}(\cdot)$ is the Stieltjes transform of the LSD of $\frac{1}{m}(\mathbf{V}_{(2)} + \mathbf{W}_{(2)})^T(\mathbf{V}_{(2)} + \mathbf{W}_{(2)})$. From Xia and Zheng (2014), the LSD of $\frac{1}{m}(\mathbf{V}_{(2)} + \mathbf{W}_{(2)})^T(\mathbf{V}_{(2)} + \mathbf{W}_{(2)})$ and $\frac{1}{m}\mathbf{W}_{(2)}^T\mathbf{W}_{(2)}$ should be the same, so that

$$\mathbf{K}_m(\ell) = -\mathbf{V}_s \cdot \ell \underline{s}(\ell) + o_{a.s.}(1)$$

where $\underline{s}(\cdot)$ is the Stieltjes transform of the LSD of $\frac{1}{m}\mathbf{W}_{(2)}^T\mathbf{W}_{(2)}$.

Therefore, almost surely, ℓ is an eigenvalue of $-\mathbf{V}_s \cdot \ell \underline{s}(\ell)$ so that

$$\underline{s}(\ell) = -1/\breve{\alpha}_j.$$

As

$$\breve{\psi}(\alpha) = \alpha + y \int \frac{t\alpha}{\alpha - t} d\breve{H}(t),$$

which is the functional inverse of the function $x \mapsto -1/\underline{s}(x)$, and $\breve{\psi}(\cdot)$ is well defined for all $\alpha \notin \Gamma_{\breve{H}}$. As a result, if such ℓ exists, ℓ must satisfy the equation

$$\ell = \breve{\psi}(\breve{\alpha}_j)$$

for some $\breve{\alpha}_j$. Furthermore, with a similar argument as in Theorems 4.1 and 4.2 of Silverstein and Choi (1995), we know that $\ell = \breve{\psi}(\breve{\alpha})$ is outside the support of the LSD $F_{y,\breve{H}}$ if and only if $\breve{\psi}'(\breve{\alpha}) > 0$.

In addition, from the proof of Lemma A.1 in Xia and Zheng (2014),

$$\lim_{p\to\infty} 3\frac{\sum_{i=1}^m |\Delta \bar{\mathbf{Y}}_{2i}|^2}{p} = \lim_{p\to\infty} 3\frac{\sum_{i=1}^m |\Delta \bar{\mathbf{X}}_{2i}|^2}{p} = \zeta,$$

where $\zeta = \int_0^1 (\gamma_t^*)^2 dt$. Then, it is easily shown that for a spiked eigenvalue α_j of the ICV satisfying $\psi'(\alpha_j) > 0$, there is an eigenvalue λ_j of $\mathcal{B}_m$ such that

$$\lambda_j \overset{a.s.}{\to} \psi_j = \psi(\alpha_j),$$

where

$$\psi(\alpha) = \alpha + y \int \frac{t\alpha}{\alpha - t} dH(t),$$

and

$$H(x) = \breve{H}(x/\zeta) \text{ for all } x \geq 0.$$

□

C Details of 92 stocks used for the US market

Table A4: List of 92 stocks in the S&P 100 index

Stock	Firm	Industry	Stock	Firm	Industry
AAPL	Apple Inc	Consumer goods	HON	Honeywell	Industrial goods
ABT	Abbott Laboratories	Healthcare	IBM	International Business Machines	Technology
ACN	Accenture plc	Technology	INTC	Intel Corp	Technology
AIG	American International Group	Financial	JNJ	Johnson & Johnson Inc	Healthcare
ALL	Allstate Corp	Financial	JPM	JP Morgan Chase & Co	Financial
AMGN	Amgen Inc	Healthcare	KO	The Coca-Cola Co	Consumer goods
AMZN	Amazon.com	Services	LLY	Eli Lilly and Co	Healthcare
APA	Apache Corp	Basic materials	LMT	Lockheed-Martin	Industrial goods
APC	Anadarko Petroleum Corp	Basic materials	LOW	Lowe's	Services
AXP	American Express Inc	financial	MA	Mastercard Inc	Financial
BA	Boeing Co	Industrial goods	MCD	McDonald's Corp	Services
BAC	Bank of America Corp	Financial	MDT	Medtronic Inc	Healthcare
BAX	Baxter International Inc	Healthcare	MET	Metlife Inc	Financial
BIIB	Biogen Idec	Healthcare	MMM	3M Company	Industrial goods
BK	Bank of New York	Financial	MO	Altria Group	Consumer goods
BLK	BlackRock Inc	Financial	MON	Monsanto	Basic materials
BMY	Bristol-Myers Squibb	Healthcare	MRK	Merck & Co	Healthcare
C	Citigroup Inc	Financial	MS	Morgan Stanley	Financial
CAT	Caterpillar Inc	Industrial goods	MSFT	Microsoft	Technology
CL	Colgate-Palmolive	Consumer goods	NKE	Nike	Consumer goods
CMCSA	Comcast Corp	Services	NOV	National Oilwell Varco	Basic materials
COF	Capital One Financial Corp	Financial	NSC	Norfolk Southern Corp	Services
COP	ConocoPhillips	Basic materials	ORCL	Oracle Corp	Technology
COST	Costco	Services	OXY	Occidental Petroleum Corp	Basic materials
CSCO	Cisco Systems	Technology	PEP	Pepsico Inc	Consumer goods
CVS	CVS Caremark	Healthcare	PFE	Pfizer Inc	Healthcare
CVX	Chevron	Basic materials	PG	Procter & Gamble Co	Consumer goods
DD	DuPont	Basic materials	QCOM	Qualcomm Inc	technology
DIS	Walt Disney	Services	RTN	Raytheon Co (NEW)	Industrial goods
DOW	Dow Chemical	Basic materials	SBUX	Starbucks Corp	Services
DVN	Devon Energy	Basic materials	SLB	Schlumberger	Basic materials
EBAY	eBay Inc	Services	SO	Southern Company	Utilities
EMC	EMC Corp	Technology	SPG	Simon Property Group	Financial
EMR	Emerson Electric	Industrial goods	T	AT&T Inc	Technology
EXC	Exelon	Utilities	TGT	Target Corp	Services
F	Ford Motor	Consumer goods	TWX	Time Warner Inc	Services
FCX	Freeport-McMoran	Basic materials	TXN	Texas Instruments	Technology
FDX	FedEx	Services	UNH	UnitedHealth Group Inc	Healthcare
GD	General Dynamics	Industrial goods	UNP	Union Pacific Corp	Services
GE	General Electric	Industrial goods	UPS	United Parcel Service Inc	Services
GILD	Gilead Sciences	Healthcare	USB	US Bancorp	Financial
GM	General Motors	Consumer goods	UTX	United Technologies Corp	Industrial goods
GOOG	Google Inc	Technology	VZ	Verizon Communications Inc	Technology
GS	Goldman Sachs	Financial	WFC	Wells Fargo	Financial
HAL	Halliburton	Basic materials	WMT	Wal-Mart	Services
HD	Home Depot	Services	XOM	Exxon Mobil Corp	Basic materials

D Details of 46 stocks used for the Hong Kong market

Table A5: List of 46 stocks in the Hang Seng index

Stock Code	Firm	Industry	Stock Code	Firm	Industry
1	CKH Holdings	Conglomerates	267	CITIC	Basic materials
101	Hang Lung PPT	Conglomerates	27	Galaxy Ent	Services
1044	Hengan Int'l	Consumer goods	291	China Res Beer	Conglomerates
1088	China Shenhua	Basic materials	293	Cathay Pac Air	Services
11	Hang Seng Bank	Financial	3	HK & China Gas	Utilities
1109	China Res Land	Financial	322	TingYi	Consumer goods
1113	CK Property	Conglomerates	3328	BankComm	Financial
12	Henderson Land	Financial	386	Sinopec Corp	Basic materials
1299	AIA	Financial	388	HKEX	Financial
135	Kunlun Energy	Basic materials	3988	Bank of China	Financial
1398	ICBC	Financial	4	Wharf Holdings	Financial
144	China Mer Hold	Services	494	Li & Fung	Services
151	Want Want China	Consumer goods	5	HSBC Holdings	Financial
16	SHK PPT	Financial	688	China Overseas	Financial
1880	Belle Int'l	Consumer goods	762	China Unicom	Technology
19	Swire Pacific	Conglomerates	823	Link Reit	Financial
1928	Sands China Ltd	Services	83	Sino Land	Financial
2	CLP Holdings	Utilities	836	China Res Power	Utilities
23	Bank of E Asia	Financial	857	PetroChina	Basic materials
2318	Ping An	Financial	883	CNOOC	Basic materials
2319	Mengniu Dairy	Consumer goods	939	CCB	Financial
2388	BOC Hong Kong	Financial	941	China Mobile	Technology
2628	China Life	Financial	992	Lenovo	Technology

References

Silverstein, J. W. and Choi, S. I. (1995). Analysis of the limiting spectral distribution of large-dimensional random matrices. *Journal of Multivariate analysis*, 54(2), 295-309.

Xia, N., and Zheng, X. (2014). On the inference about the spectra of high-dimensional covariance matrix based on high-frequency noisy observations. *arXiv: 1604.03638*.

Yao, J., Bai, Z., and Zheng, S. (2015). Large Sample Covariance Matrices and High-dimensional Data Analysis. *Cambridge University Press*.